GEOPHYSICAL SURVEYS OF DEBRIS FLOW SUSCEPTIBLE AREAS;

IMPLICATIONS FOR RISK PERCEPTION

A Thesis

by

DANIEL THEODORE TEBO

Submitted to the Office of Graduate and Professional Studies of
Texas A&M University
in partial fulfillment of the requirements for the degree of

MASTER OF SCIENCE

| | |
|---|---|
| Chair of Committee, | Mark E. Everett |
| Committee Members, | Douglass Shaw |
| | John R. Giardino |
| Head of Department, | Michael Pope |

August 2016

Major Subject: Geophysics

# ABSTRACT

Understanding how an individual cognizes and processes geophysical information pertinent to natural hazards can further enhance geophysical imaging in becoming more reliable and beneficial to the public. It has long been debated to what degree an individual's perception of the risk associated with natural disasters changes with the level of exposure to relevant scientific evidence and the manner in which the information is communicated by experts. Debates on this topic have circled around climate change, natural hazard preparedness, and health risks. One situation that lends itself to studying the public perception of the information content in geophysical images is debris flow hazard in inhabited mountainous regions, as such flows have an immediate impact on human life, property and amenity values.

Geophysical mapping was performed along the Front Range in Boulder County, Colorado, to provide information about the potential for new additional debris flows in light of the September 2013 flooding episodes, which brought a State of Emergency to Boulder County. The geophysical maps provided subsurface images of geotechnical proxies that are herein interpreted in terms of debris flow susceptibility along a given profile. We acquired two along-slope and two down-slope electrical resistivity tomography (ERT) profiles for assessment of potential slope failure.

The ERT images suggest a complex subsurface heterogeneity characterized by shallow localized channels of high hydraulic conductivity constrained by surrounding areas of low hydraulic conductivity. Understanding the geotechnical implications of these

ii

subsurface structures gives better insight into the apparent risk of future rainfall-induced debris flows in this specific area.

The geophysical information ideally would be widely communicated to the public and local stakeholders for risk assessment and mitigation purposes.  In this study, instead we have used a small informal focus group approach which has provided a crude indication of the potential response of the public and stakeholders to the information content revealed in the ERT images pertaining to Boulder county debris flow-susceptible slopes. Particularly, we monitored changes in expressed risk perception as various levels of scientific information were systematically revealed to the focus group.  The focus group study is a precursor to a larger study in understanding how the general public perceives geophysical information regarding natural hazards and its implications for hazard mitigation.

# ACKNOWLEDGEMENTS

A special thanks to my committee chair, Dr. Everett, and committee members, Dr. Shaw and Dr. Giardino for guiding me through this research project. It was a journey of personal growth and achievement.

I would also like to thank Akhil Amara and Dr. Everett for helping me with the drudgery of collecting ERT data along the slopes in Boulder, Colorado, as well as family and friends for their support throughout my time at Texas A&M University.

# NOMENCLATURE

| | |
|---|---|
| ERT | Electrical Resistivity Tomography |
| SRC | Spatial Resistance Change |
| $V$ | Voltage (volts) |
| $E$ | Electric Field (volts/meter) |
| $J$ | Current Density (amperes/meter$^2$) |
| $Z$ | Impedance (ohm) |
| $\rho_a$ | Apparent Resistivity (ohm-meter) |
| $\rho_a^H$ | Apparent Resistivity calculated with an array type (ohm-meter) |
| $\sigma$ | Electrical Conductivity (Siemens) |
| $I$ | Current (amperes) |
| $r$ | Radius (meters) |
| $\pi$ | Pi |
| $k$ | Geometric Factor (ERT array configuration) |
| $n$ | Data level (array configuration) |
| $a$ | Electrode Spacing |
| $u$ | Response to forward problem |
| $F[m]$ | Physics that governs the forward problem |
| $m$ | Earth Model |
| $R_1$ | Model Roughness |
| $X^2$ | L$_2$ error norm (chi squared) |

| | |
|---|---|
| *W* | Data covariance matrix |
| *d* | Data vector |
| *U[m]* | Unconstrained functional |
| $J_i$ | Jacobian Matrix |
| *μ* | Lagrange Multiplier |
| *k* | Wave number (Fourier Transform) |
| *Δρ* | Spatial change in resistivity |
| *T* | ERT sensitivity response function |
| *S* | ERT Sensitivity function |
| *P* | Perturbation properties of model sensitivity |
| *CS* | Cumulative model sensitivity function |

# TABLE OF CONTENTS

Page

LIST OF FIGURES

# LIST OF TABLES

# 1. OBJECTIVE AND INTRODUCTION

OBJECTIVE

This thesis project consists of assessing the cognition and processing of geophysical information, as it is introduced to members of the public. The over-arching ambition of the research is to improve the utility of geophysical information for natural hazard risk assessment. The information in this project is specific to debris flows in proximity to the city of Boulder, Colorado. In such areas of steep topography, susceptibility of rainfall-induced debris flows to down-slope real assets is an important concern. Debris flows create hazardous situations that can cause destruction to property and sometimes life. Many times, debris-flow hazards are overlooked by the general public, who are unaware or only marginally aware of the associated destructive forces. This inattention leads to a civil concern in which mitigating these risks becomes problematic. However, identification of hazardous areas is challenging on steep slopes where deployment of traditional geotechnical testing equipment is cumbersome and costly.

Geophysical maps provide a low cost, easily manageable way to image the subsurface in such cases. The advantage of geophysical techniques is that they provide the public with information to perform assessments of debris flow hazard in an inexpensive and timely manner. To determine the optimal level of technical detail that this information should contain, a public perception survey can be employed. A survey provides insight into how an individual's perceived risk of the occurrence and destructiveness of such natural

hazards changes upon exposure to geophysical information as it is explained in increasing detail by an expert.


INTRODUCTION

The terms "landslide" and "debris flow" often disseminate through the general public as mutually exclusive events as a result of the lack of understanding between the nature and mechanisms involved. Within the scientific community, the terms describe events that are physically different, but with the possibility of being functionally dependent. Generally, landslides are defined as the down-slope movement of a disjointed solid mass of sediment and rock. Whereas, a debris flow is a moving, fluidized mass of loosely packed sediments, rock and debris, typically originating from a landslide. Once the landslide mass loses cohesion as a result of a loss of particle friction, it begins to fluidly flow as a debris flow. For this study, the term "landslide" will be excluded, and "debris flow" will be inclusive of both events.

Debris flows have historically been connected with economic loss and ultimately loss of life (e.g., Oso, WA 2014; Veracruze, Mexico 1920; Chittagong, Bangladesh 2007; etc.) (Mejía-Navarro 1994). Regions with relatively steep topography and subject to large rainfall events are often susceptible to catastrophic debris flow events. Many such areas have undergone rapid development whereas debris flow susceptibility assessments and the associated risk communication have not been heeded (Jakob and Hungr 2005). The historical incidence and susceptibility of debris flows within the United States is shown in

Figure 1.1. Mountainous regions in the west, and areas within Appalachia and along the west coast are most susceptible to debris flows. Intrinsically, many of these areas have also become hotspots for development of new residential communities and businesses.
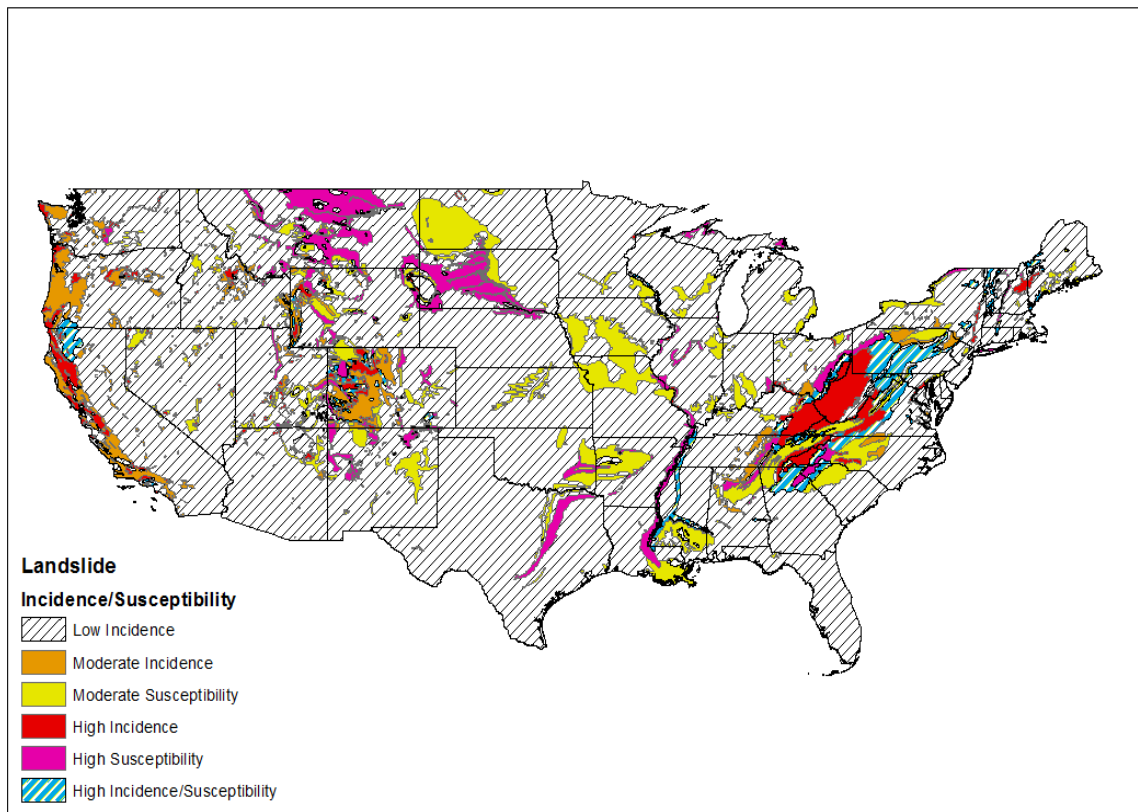


*Figure 1.1: Landslide incidence and susceptibility map of the United States (adapted from Radbruch-Hall et al. 1982, USGS).*

This project focuses on one specific debris flow event located near the city of Boulder, a popular tourist destination of great scenic beauty endowed with abundant

outdoor recreational amenities, located on the front range of the Rocky Mountains. During

the month of September 2013, Boulder experienced record rainfall estimated to have been

a 100-year flood event (Coe *et al.* 2014) (Figure 1.2).
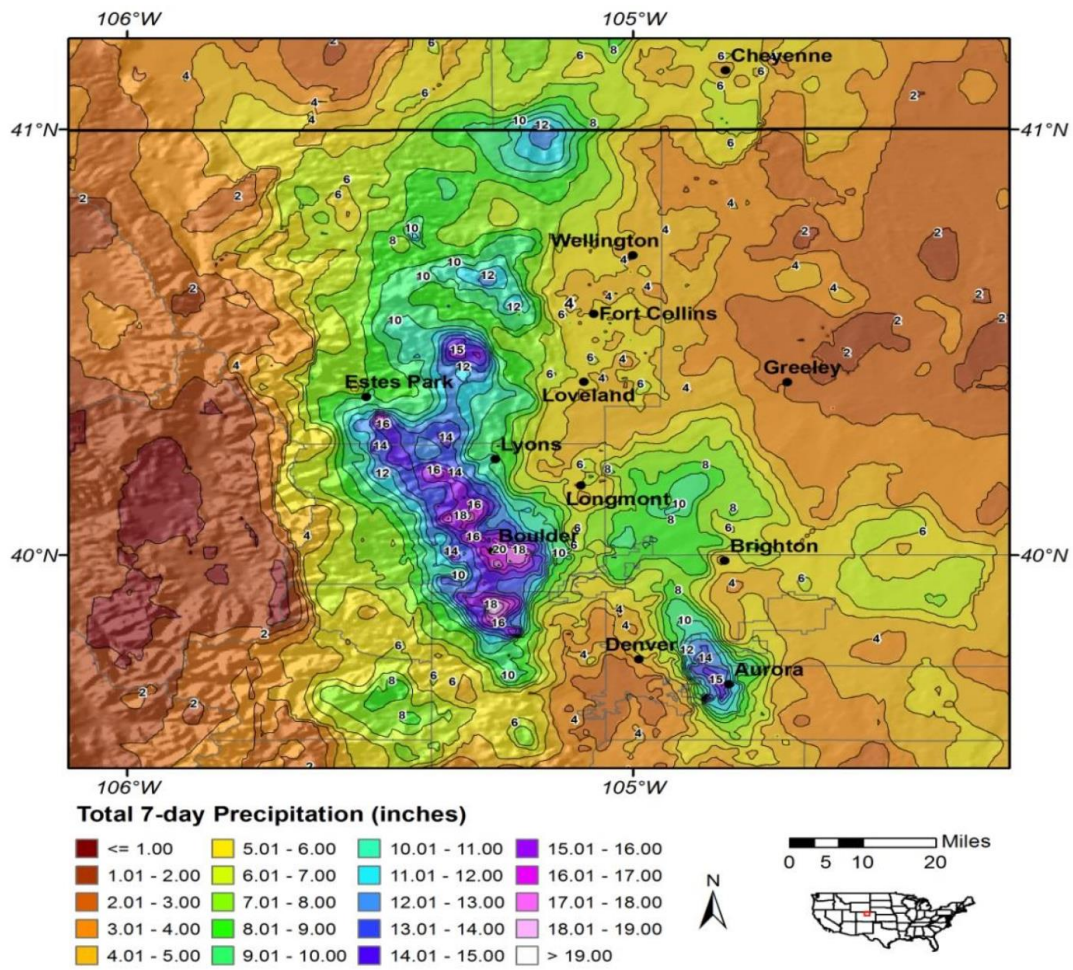


*Figure 1.2: Colorado rainfall analysis of September 9-16, 2013. Precipitation in inches for the total 7 – day period (Vallee 2014).*

The storm began on September 10th, with peak flooding on September 11th and 12th (Figure 1.3). Much of the resulting damage to homes, businesses and infrastructure was due to the overland floodwater. A swarm of destructive, unexpected debris flow events also occurred (Figure 1.4). The debris flows were the result of soil supersaturation because of the antecedent rainfall.
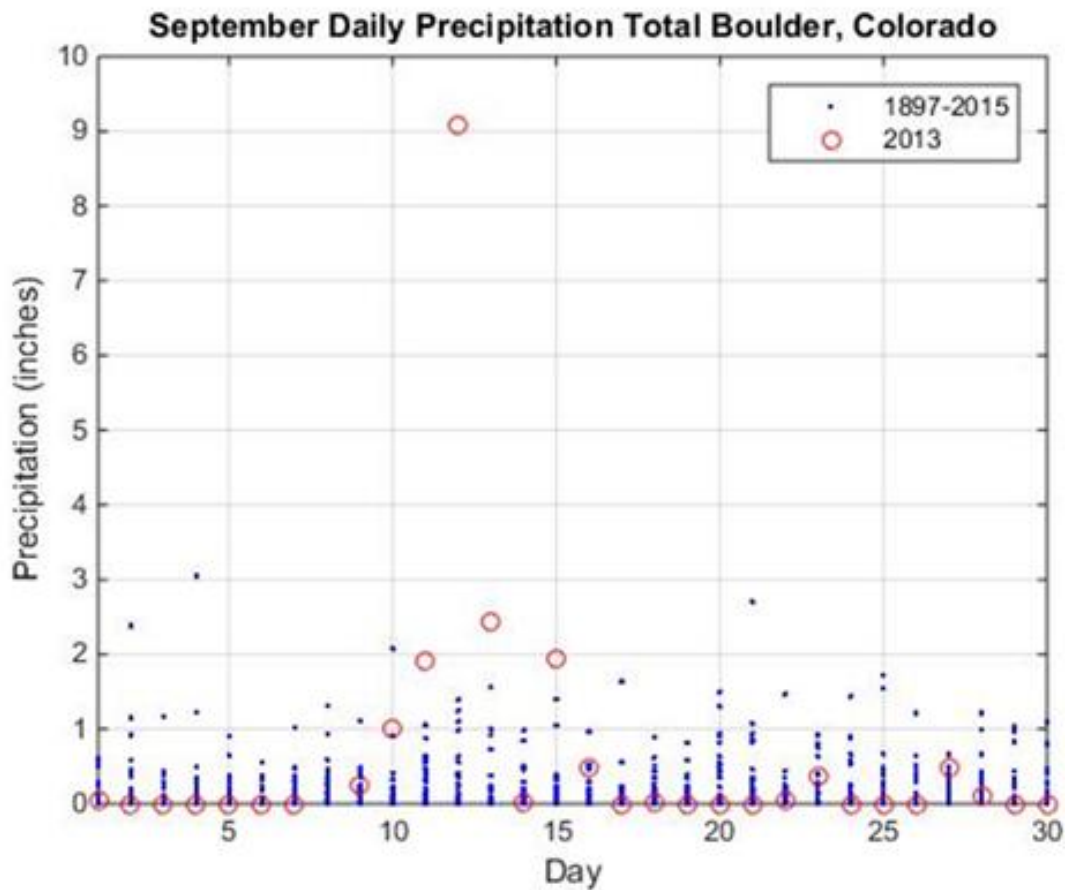


*Figure 1.3: September yearly flooding totals. The September 2013 flooding event is highlighted in red and all other years are shown in blue (data attained from NOAA).*

Loss of life ensued in a few cases as the result of the swiftness of these debris flows.  Most of the downslope residents of Boulder were unaware of a debris flow hazard, and were most likely concerned only about the overland floodwater.
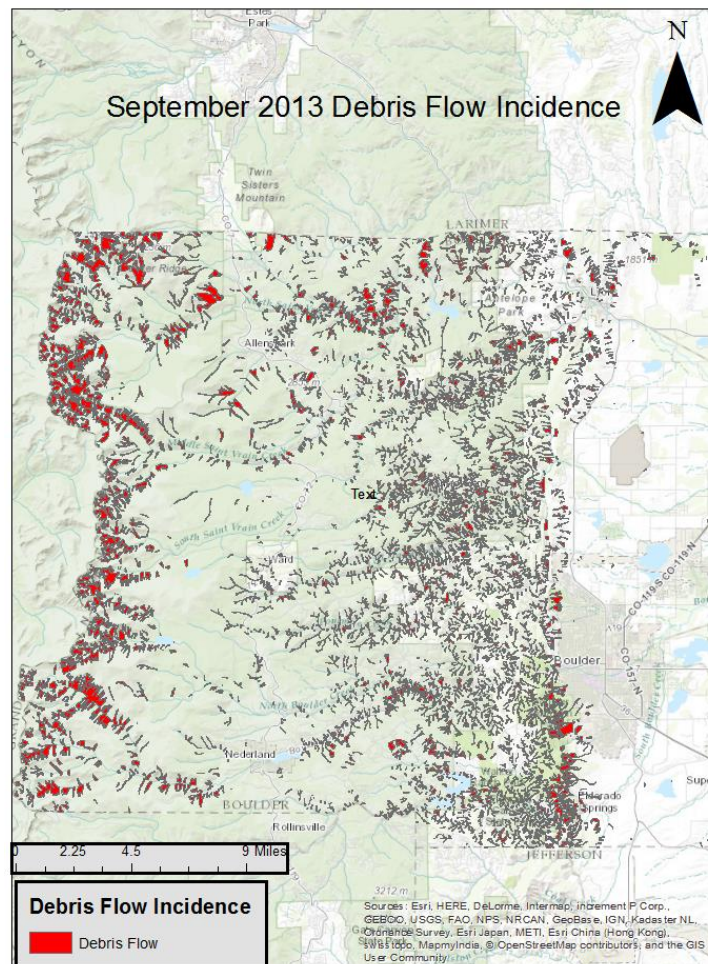


*Figure 1.4: September 2013 debris flow incidence map for Boulder County, Colorado (USGS n.d.).*

Debris flow mobilization is the result of gravitational potential energy becoming rapidly converted to internal kinetic energy, resulting in a transformation from slow movement on a localized sliding surface to widespread chaotic deformation (Iverson *et al.* 1997). Failure surfaces associated with a sliding mass of sediment, water and rock can range from well-defined to heterogeneous and multi-faceted. The failure surface geometry can be linked to the cohesion of grain-to-grain interactions that occur within the sediment and rock. In soil mechanics, the Coulomb criterion prescribes conditions for failure in terms of the driving and resisting shear stresses acting on a specific volume of sediment and rock (Anderson and Jackson 1992). When the resisting shear stress becomes less than the driving shear stress, a failure surface initiates. Most commonly, water within the sediment volumetric pore space controls the cohesion of grain to grain interactions. When water is not adequately drained following its infiltration, the pore pressure increases. Excess pore pressure is generally a major controlling factor in the initiation of a failure surface (Ellen and Fleming 1987). Consequently, most debris flows occur during extreme rainfall events. Once a failure surface initiates, the mass of sediment, rock and water begins to move while grain to grain cohesion continues to decrease. Debris can flow long distances within shallow crevasses in the topography, often with destructive and sometimes with catastrophic force (Benda and Cundy 1990).

Because many debris flows occur in areas of steep topography, where traditional geotechnical equipment is costly and cumbersome to deploy, indirect subsurface mapping tools have become invaluable (Godio 2006). Traditionally, geotechnical equipment is used

to gather field samples for laboratory analysis which leads to the assessment of a debris flow susceptible area based on the specific locations where the samples were taken. The equipment needed to do the analysis requires experienced and oftentimes licensed professionals to run (drilling, laboratory testing, etc.) which greatly increases the time and cost of the project. However, with rapid development of formerly remote mountainous regions, the need for inexpensive and quick methods to evaluate debris flow hazards is becoming essential.

Many geophysical techniques can be used to evaluate debris flow susceptibility; in particular, one such technique, electrical resistivity tomography (ERT), has become widely used for its ability to reliably image complex subsurface geology (Perrone *et al.* 2014) (Dahlin 2001). ERT data acquisition and production of a subsurface image does not require extensive training. Identifying debris flow susceptibility areas is an important step to mitigation, and communicating the hazard to inhabitants is critical. This is why ERT, with its ease of use and contiguous areal coverage, is seen as an important advance. Studies have shown that effective communication with the public increases the likelihood of success of a hazard management plan. Steelman *et al.* (2012) noted when risk was effectively communicated prior to an event, the public accepted a more flexible risk management plan. Being better prepared for a potentially harmful event will ultimately mitigate the resulting loss of life and property. The research goal is that ERT geophysical images and their interpretation would become a standard part of a debris flow risk communication strategy.

To better communicate technical information regarding risks, an understanding of an individual's cognition of this information is necessary. In general, varying the degrees of technical information introduced to the public can have multiple effects. If an individual is introduced to technical information that is beyond their understanding, he or she may ignore such information. Moreover, if an individual is introduced to confusing or otherwise unclear information, he or she may also discard such information. It is also important to understand how individuals act when presented with risks of differing outcome severity and occurrence probability. Kunreuther *et al.* (2001) noted that in circumstances which the outcome severity is low with a high occurrence probability as compared to those characterized by a high outcome severity with a low occurrence probability, an individual may perceive and act on these risks with entirely different behaviors. These effects ultimately make it difficult to determine the best societal decisions regarding natural hazards. This situation motivates the development of a better understanding about how emerging technical advances, such as ERT geophysical methods, can be used in communication strategies that educate the general public on apparent risks associated with debris flows.

This thesis will first introduce the ERT method that is used to perform the geophysical mapping, along with a short description of the geology of the Boulder Front Range study area. The results of the ERT analysis will then be discussed. Risk perception of debris flows will then be discussed in general terms, followed by a description of the risk perception survey provided to a small focus group (IRB2016-0284D) and, finally, implications of the results of the survey.

## 2. GEOLOGIC SETTING

## GEOLOGIC SETTING

Boulder County is located within the transition zone between the Great Plains and the Rocky Mountains, a region in which sedimentary rocks are juxtaposed against metamorphic and igneous rocks in many places. During the time of the late Cretaceous Seaway, coastal environments were dominant along what is now the eastern margin of Colorado. These low-energy environments hosted the deposition of sedimentary layers such as sandstone, limestone, shale and occasional beds of coal (Figure 2.1) (Bridge 2004).
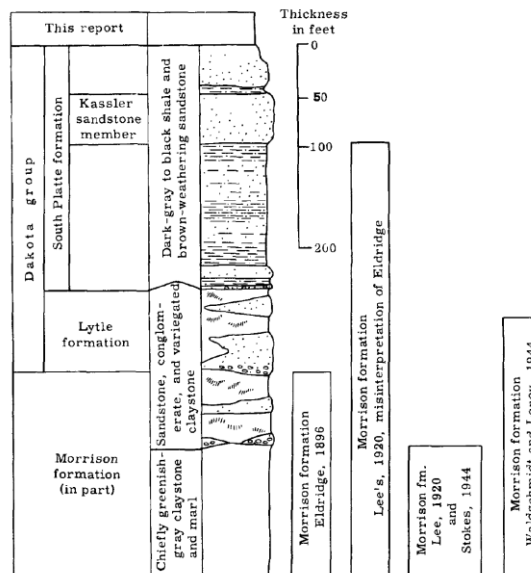


*Figure 2.1: Generalized stratigraphic column depicting the geology of the Colorado Front Range (Waagé 1955).*

As the late Cretaceous Seaway began to retreat to the northeast, uplift and tilting ~70 Ma associated with the Laramide orogeny began building the Rocky Mountains. Extensive deformation due to mountain building and magmatic intrusions become a dominant feature of the growth of the Rocky Mountains. The neighboring transition zone between the Great Plains and the current Rocky Mountains is characterized by uplift and tilting of the Cretaceous Seaway deposits along with remnants of the ancestral Rocky Mountains (Figure 2.2). Presently, the tilted sedimentary formations are exposed as hogbacks along the eastern front of the Rocky Mountains.
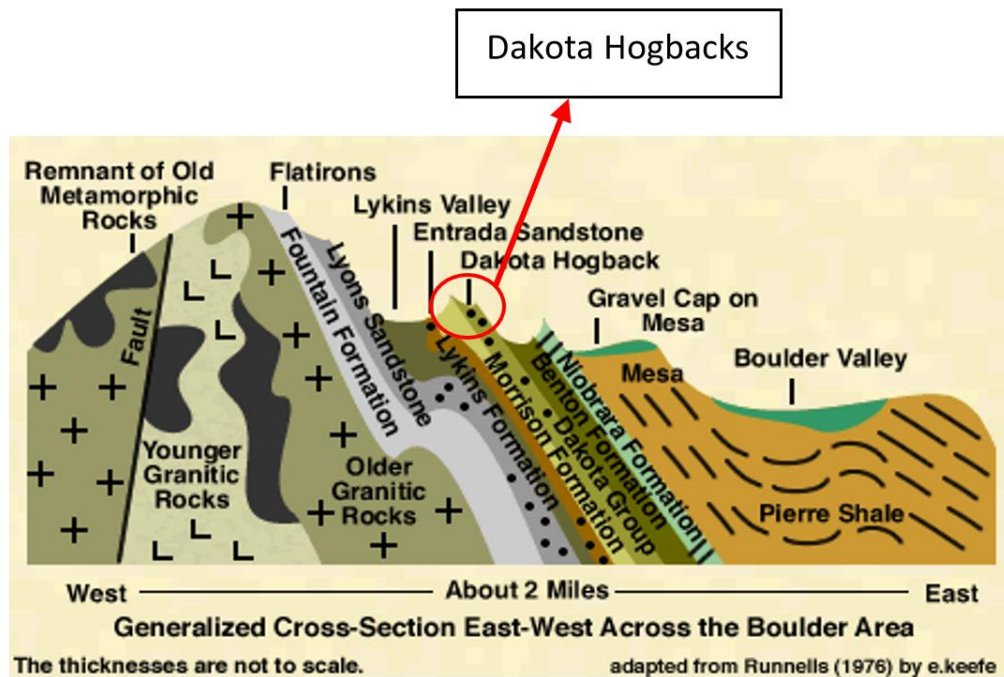


*Figure 2.2: Generalized cross section of the Boulder, Colorado area depicting the uplift and tilting of the Colorado Front Range (Runnells 1976).*

The research area is located within the Dakota group consisting of interbedded marine shales and sandstones, deposited during the late Jurassic on top of the Morrison group. The Dakota group is divided into two formations, the marine South Platte Formation overlain by the Pierre Shale, and the underlying non-marine Lytle Formation (Braddock 1962). The Lytle Formation consists of conglomeratic sandstone and interbedded variegated mudstone with a thickness ranging from 15-25 m. Above the Lytle Formation, the South Platte Formation consists of an upper sandstone unit ~10-25 m thick with a middle shale unit of ~46 m thickness of dark-grey shale, and a lower 10 m thick sandstone unit called the Plainview Sandstone Member (including the Kassler Sandstone Member). The Dakota group is exposed as two hogbacks with north-striking ridges and valleys (see Figure 2.2). The western hogback is formed from the Lytle Formation and the South Platte Plainview Sandstone Member. The valley between the hogbacks consists of the middle shale unit of the South Platte Formation. The first sandstone member of the South Platte Formation makes up the eastern hogback (Waagé 1955).

# 3. ELECTRICAL RESISTIVITY TOMOGRAPHY

## BASIC THEORY AND CONCEPTS

The efficacy of the transfer of electrical energy by means of the migration of ionic charge carriers through a soil, rock and pore water mass is governed by the electrical conductivity. The electrical conductivity is controlled by factors in three categories: phases of the soil matter (solid, gas, liquid), solid volume quantifiers (particle shape, orientation, size, and cation exchange potential between the solid matrix and the pore fluid (Figure 3.1)) and environmental factors (soil temperature, and the ionic strength and cation composition of the pore fluid) (Freidman 2005) (Tabbagh *et al.* 2002).
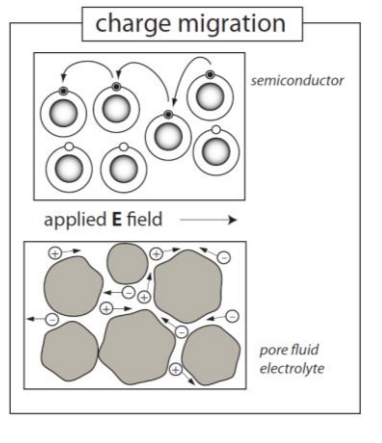


*Figure 3.1: Electrical charge migration pathways shown by direction of applied electric field (Everett 2013).*

These factors together determine the electrical potential raised between two electrodes, where the intervening soil/rock and pore fluid volume acts as an equivalent resistor. Knowledge of the soil and rock electrical conductivity can reveal subsurface information relevant to debris flows, including the clay content and lithological boundaries (Merritt 2016; Bogoslovsky 1977).

Many case studies have been performed in which ERT is the principal geophysical tool used to evaluate landslide morphology and past occurrence. Lapenna *et al.* (2005) found the ERT method to be particularly useful for identifying geometric boundaries of complex earthflows in the Basilicata region, Italy. These landslides were controlled by hydrogeological conditions in which groundwater movement played a key role in the formation of slip surfaces. One of the fundamental parameters that emerges from ERT analysis of landslide-affected regions is the subsurface spatial variation in resistivity – this parameter is often indicative of a change in lithology. In many cases, a spatial change in resistivity represents the boundary of a conductive/resistive anomalous zone caused by an area of possible clayey, or otherwise hydraulically constrained lithology (Dostál *et al.* 2014). In cases where rainfall is the principal factor controlling slip surface (shear surface) formation, these lithological conditions become the primary locations at which a slip surface could eventually form. Slip surfaces form when the pore water pressure increases substantially, thus creating a loss of cohesion between grain particles (Carey and Petley 2014). Increased pore pressure may be produced by rainfall infiltration into the subsurface at locations where drainage is not adequate (Erginal *et al.* 2008). To better understand the

role of ERT in generating subsurface images from which the locations of slip surfaces can be inferred, the fundamental theory of this geophysical technique is first reviewed.

Generally, an electric current (I, amperes) is injected into and withdrawn from the subsurface through a pair of electrodes. The source and sink of current generate a voltage (V, volts). The latter is measured between a second pair of electrodes. The subsurface distribution of the current as it is injected into and withdrawn from the subsurface is radially symmetric in the immediate vicinity of the injection and withdrawal electrodes (Figure 3.2).
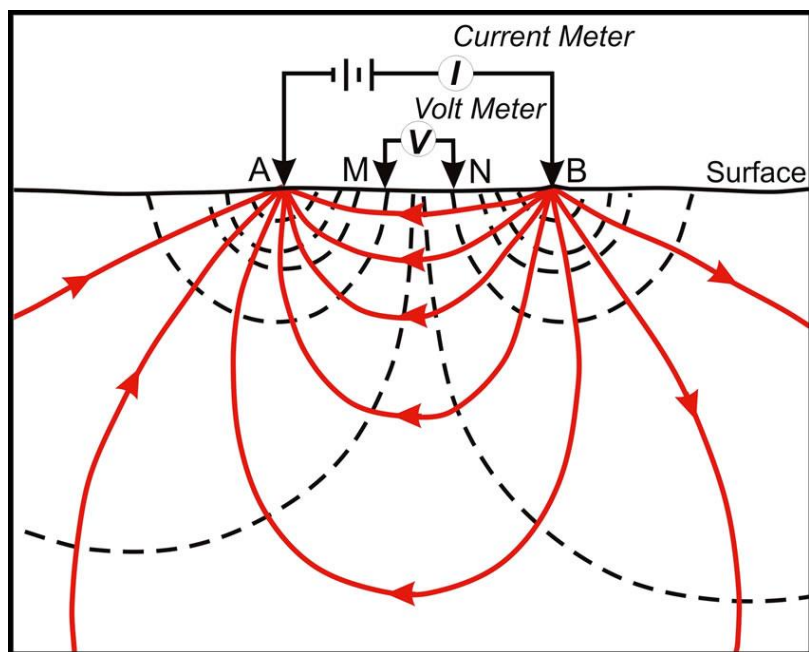


*Figure 3.2: Arrow and equipotential lines plot showing electric field direction with current and potential electrodes (Clark and Page 2011).*

The associated electric field (E) is related to the subsurface current density ($J$) by:

$$J = \sigma E \tag{3.1}$$

$$E = -\nabla V \tag{3.2}$$

$$J = -\sigma \nabla V \tag{3.3}$$

with $\sigma$ being electrical conductivity (S, siemens). If the subsurface is represented as a halfspace of uniform resistivity, the current extends radially outward from the source and sink, and the current density $J$ becomes:

$$J = \frac{I\hat{r}}{2\pi r^2} \tag{3.4}$$

where $\hat{r}$ is a radial unit vector. The voltage V at a specific point A (Figure 3.2), with respect to an arbitrary point at infinity, is equal to the work done by the electric field E in moving a unit charge from the point at infinity to location A. The voltage, therefore is an integral of the product of electric field and distance, given by:

$$V = \int_r^\infty E \cdot dr = \int_r^\infty \frac{I\rho}{4\pi r^2} dr = \frac{I\rho}{4\pi r} \tag{3.5}$$

with $\rho = 1/\sigma$ (resistivity). The voltage difference between two points A and B located on a uniform halfspace of resistivity $\rho_a$ is simply (Figure 3.2):

$$V_{AB} = V_A - V_B = \frac{I\rho_a}{2\pi}[\frac{1}{r_A} - \frac{1}{r_B}] \tag{3.6}$$

and rearranging for the "apparent" resistivity ($\rho_a$) of the halfspace:

$$\rho_a = \frac{2\pi V_{AB}}{I}[\frac{1}{r_A} - \frac{1}{r_B}]^{-1} = kZ \tag{3.7}$$

Apparent resistivity represents the ERT measurement, associated with a given pair of electrodes, and made at a specific time. Apparent resistivity can be simplified using the electrode-array geometric factor (k) and earth's impedance (Z), the latter being shown generally by:

$$Z = \frac{V}{I}$$

(3.8)

such that

$$\rho_a = kZ$$ (3.9)

The geometric factor $k$ is dependent upon the electrode array configuration (see ACQUISITION). It is important to keep in mind that the above equations are formulated assuming a homogeneous, isotropic subsurface halfspace.

Electrical resistivity soundings were traditionally collected using a four electrode array configuration (Schlumberger, Wenner, dipole-dipole, etc.) (Dahlen 2001). The different arrays have different trade-offs between lateral resolution and depth penetration (Everett 2013). However, the traditional electrode configurations are cumbersome to deploy and, in practical terms, are capable of providing only a simple representation of the subsurface geology. Their inability to accurately image complex subsurface geology led to the search for more sophisticated data acquisition protocols using advanced electrode arrays. Daily and Owen (1991) pioneered such a methodology, introducing electrical resistivity tomography (ERT) using cross-borehole profiling. Their technique used a multielectrode - multichannel acquisition system to gather electrical resistance soundings through sequential energization of different pairs of injection and withdrawal electrodes.

Laboratory studies of the electrical properties of soil and rock has led to an estimated range of resistivity values as a function of lithology and water saturation (Loke 1999) (i.e. wet or dry end-members). The near-surface soil and rock encountered in the Boulder front-range area consists of clay, colluvium, sandstone and shale. The corresponding ranges of electrical resistivity values, for wet and dry conditions, are shown in Table 1.

| Material | Resistivity (ohm-m) wet-dry |
|---|---|
| Clay | 1-100 |
| Colluvium/Alluvium | 10-1000 |
| Sandstone | 10-1500 |
| Shale | 30-1200 |

*Table 1: Electrical resistivity properties of common subsurface materials (adapted from Loke 1999).*

SURVEY LOCATION
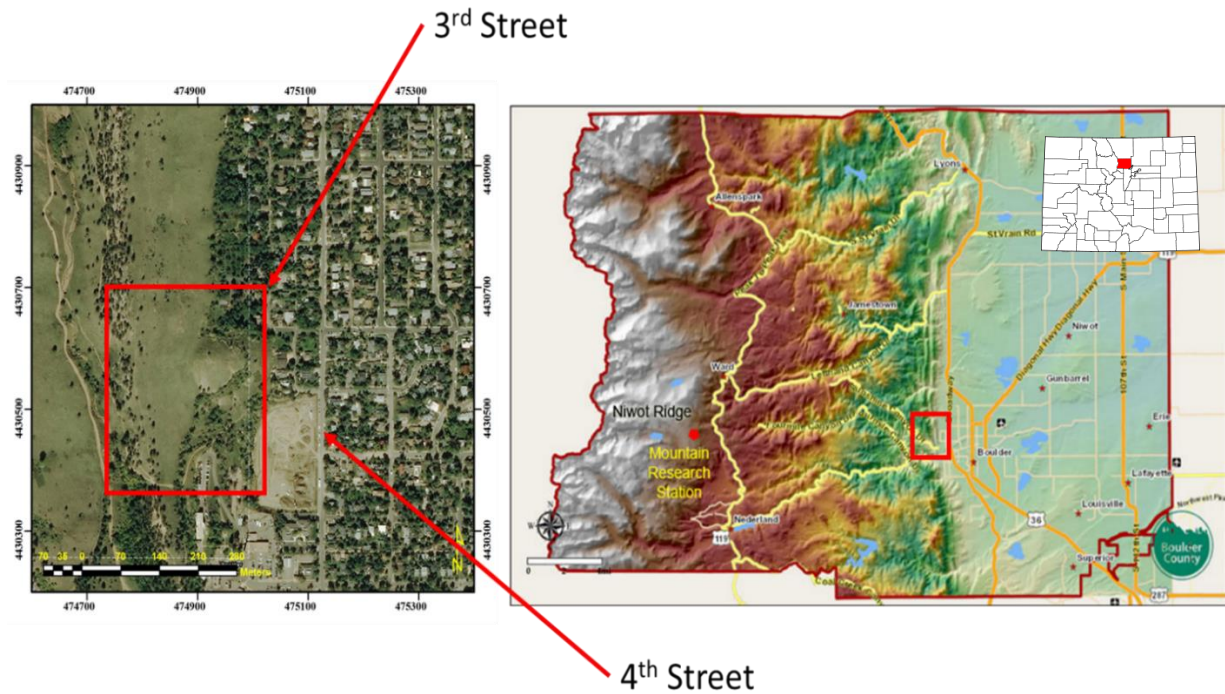


*Figure 3.3: Location of survey west of 3<sup>rd</sup> and 4<sup>th</sup> streets in Boulder, Colorado. Inset in Boulder County image is the extent of the State of Colorado (Adapted from ESRI Imagery 2015 and Boulder County n.d.).*

The research area is located on the slopes west of 3rd and 4th streets in Boulder, Colorado (USGS Boulder Quadrangle; see Figure 3.3). This area is within the region affected by the September 2013 flooding event that occurred along the Colorado Front Range (Coe *et al.* 2014). Contained within this area are hiking trails, businesses, homes

and roads.  Colorado Open Spaces oversees land management within the research area and assigned the permit that made the geophysical fieldwork possible.

Two along-slope and two downslope ERT transects were performed on March 27–30 2015, as shown in Figure 3.4. The two downslope transects and the upper along-slope transect were deployed using an electrode spacing of 2 m. The lower-along slope transect was performed with 3 m electrode spacing with the aim of probing deeper to the bedrock.
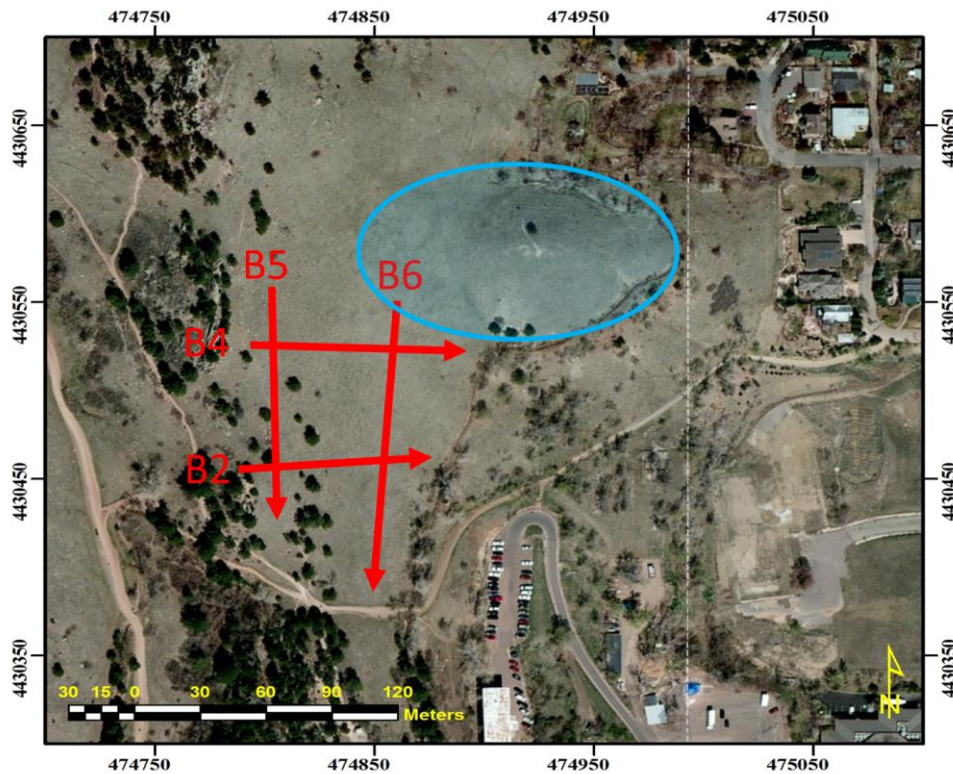


*Figure 3.4: Locations of ERT transects along slope west of 3<sup>rd</sup> and 4<sup>th</sup> streets in Boulder, Colorado.  Blue oval indicates historic landslide remnants (ESRI Imagery 2015).*

ACQUISITION

Briefly, the geophysical instrumentation used for this project comprises the AGI R8/IP SuperSting® Earth Resistivity Meter (Figure 3.5), connected to a 12-volt battery source.



*Figure 3.5: Photo of AGI R8/IP SuperSting® Earth Resistivity Meter connected to 12 volt deep cycle battery (image by Suwimon Udphuay).*

The user instructs the control unit to inject a current through one of an arrangement of electrodes (12-inch steel rods) and receive the returning current through another of the electrodes, forming a current source/sink pair. The user specifies a sequence of such current/sink pairs to be used in order to gain good lateral coverage beneath the electrode layout. The array configurations used for this survey are the Wenner and Schlumberger arrays, the acquisition sequence was set using AGI EarthImager Software®. This array combination is known to provide a good compromise between vertical and horizontal resolution suitable for mapping complex subsurface geology (Loke 1999). The geometric factor *k* (equation 3.9) used for the Wenner and Schlumberger array to calculate the apparent resistivity is shown by:

$$k = \pi n(n+1)a \quad \text{(Schlumberger)} \tag{3.10}$$

$$k = 2\pi a \quad \text{(Wenner)} \tag{3.11}$$

where *n* is the data level and *a* is the electrode spacing (see Figure 3.6 for the Schlumberger and Wenner protocol).
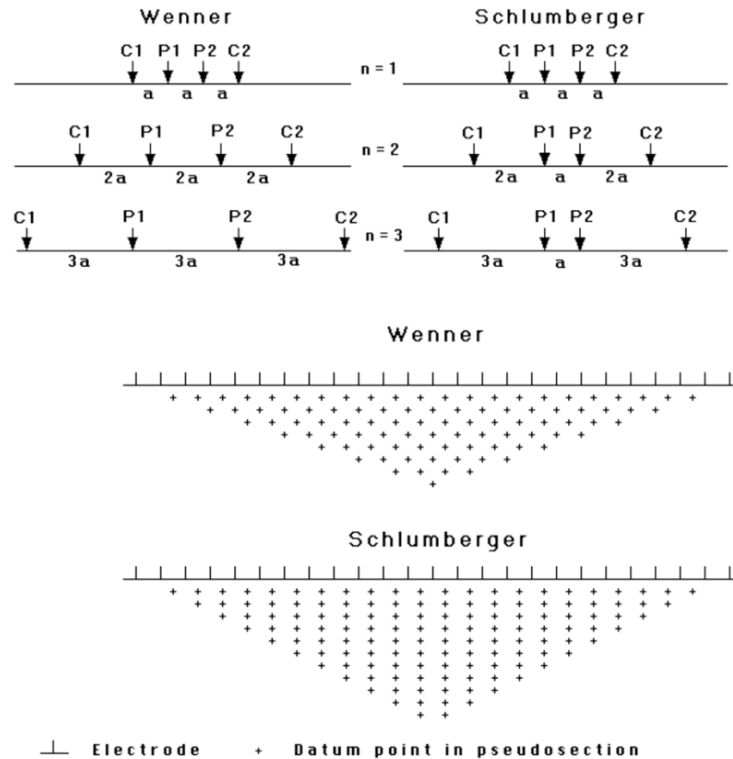
*Figure 3.6: Wenner and Schlumberger arrays where a is the electrode spacing, and n is the data level. Datum points are shown as crosses below the surface (Loke 1999).*

Acquisition proceeds across the array; as each data level is completed, the data level increases by one and acquisition across the array is repeated. The electrode spacing is multiplied by the data level. The resulting measurements are assembled into a two-dimensional apparent resistivity pseudosection. The apparent resistivity is assigned to a depth and lateral position dependent on electrode spacing and location, respectively, with model sensitivity dependent on array type.

Figure 3.7 shows variations in model sensitivity for the Schlumberger array using 1 m electrode spacing at data level *n=3*. Model sensitivity is a function of the spatial

averages of resistivity distribution that is defined by the magnitude in perturbation in the

voltage distribution due to a small perturbation in subsurface resistivity distribution

(Everett 2013). To show this mathematically, where $T$ is the response function defined as:

$$T = \frac{(\rho_a - \rho_a^H)I}{k}$$
(3.12)

with $\rho_a^H$ representing the apparent resistivity measurement calculated without the array

type, and apparent resistivity $\rho_a$ (ohm-m) calculated with the array type. $I$ (amperes) and $k$

represent the current and geometric factor, respectively (Furman *et al.* 2003). Using the

response function $T$, model sensitivity $S$ can be measured by the magnitude of the

response, shown by:

$$S(P) = |T|$$
(3.13)

The vector representing the perturbation properties (location, size, and relative electrical

conductivity) is shown by $P$. To show the sensitivity distribution spatially, a summation of

the sensitivities $S$ can be shown cumulatively by:

$$CS = \frac{\sum_{i=1}^{j} S}{\sum_{i=1}^{N} S}$$
(3.14)

Figure 3.7 shows this sensitivity function in a 2-dimensional map of the Schlumberger

array configuration.

*Figure 3.7: Sensitivity function plot for the Schlumberger array. Sensitivity values are highest nearer to the surface along with vertical and horizontal resolution (Loke 1999).*

INVERSION

Inversion is used in this study for subsurface resistivity model construction. Generally, geophysical inversion is used to acquire images of Earth's subsurface based on indirect, sparse and noisy measurements (in this case, apparent resistivities determined from voltage readings across pairs of electrodes). An inversion is based on repeated calls to a forward-modeling algorithm that predicts the response of an assumed model of the subsurface. The forward problem is specified by an Earth model m(r) for which we can calculate the response u(r). The forward-modeled response is then compared to the observed response, the latter reflecting the actual subsurface physical properties at the time of measurement. The computed responses can be represented by the simple equation:

$$u = F[m] \qquad\qquad (3.15)$$

where F contains the physics that governs the forward problem (in this case, it is essentially Ohm's law plus the law of conservation of charge), m is the Earth model (in this case, the subsurface resistivity distribution) and u is the Earth response (in this case, the apparent resistivities) to the geophysical excitation. An overview of geophysical inversion is provided in Everett (2013). The objective of the inversion process is to find a model that is characterized by a desired attribute, such as smoothness, while fitting the observed data to a specified tolerance. In many cases, there is little or no known information about the subsurface prior to inversion. In order to find a good-fitting model with the desired attribute, iterations amongst such models are needed to reduce the misfit between the observed and calculated model responses. Many of the geophysical

inversion methods used today can rapidly attain convergence to a suitable model with a low misfit. Thus, it becomes somewhat a subjective matter to select a particular method for inversion. Many inversion algorithms, including conjugate gradient, least-squares, maximum entropy, simulated annealing, artificial neural networks and singular value decomposition, use different search strategies to achieve convergence (Loke *et al.* 2003). Regularized least squares is a versatile method that allows the user to include a priori information in the inversion process, or to attach a desired attribute to models. The two most widely-used regularized least squares inversion algorithms for 2-D ERT are "smooth" and "robust, or blocky". In smooth inversion, the desired attribute is smoothness of the subsurface physical property being imaged (Boonchaisuk *et al.* 2008). In blocky inversion, sharp contrasts in physical properties are favored. Both of these algorithms rapidly converge to a low misfit between the observed and calculated responses.

In areas where complex geology is expected, smooth model inversion is often preferred over blocky inversion since, in these cases, there are too many sharp contrasts to resolve them all properly. Figure 3.8 shows a comparison between blocky and smooth reconstruction of a rectangular prism containing a smooth boundary transition zone to the background. In this case, the smooth model inversion performs better since the true model has a gradual contrast.

For this thesis project, the Quasi-Newton (QN) nonlinear smoothness-constrained least squares inversion method is selected because of its rapid convergence and relative insensitivity to noise (Loke *et al.* 2003). The QN algorithm produces the smoothest
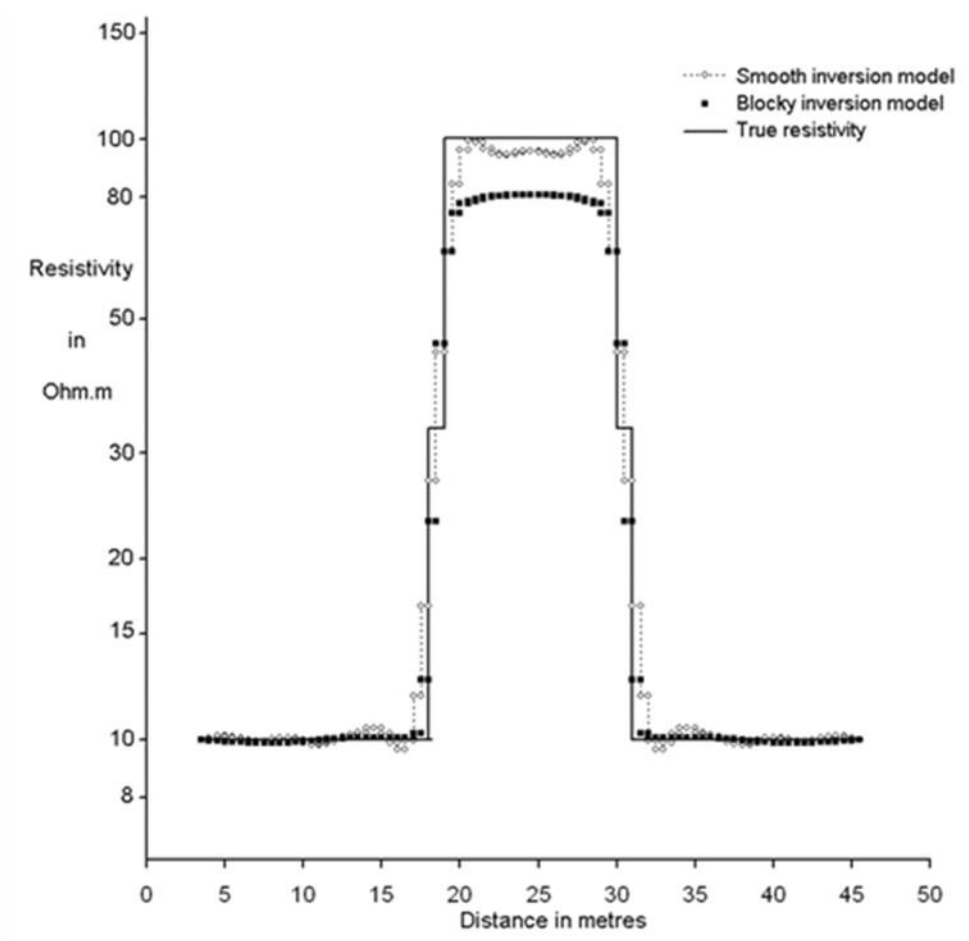
*Figure 3.8: Smooth vs. blocky inversion model comparison to true model with a boundary layer introduced within a prism (Loke et al. 2003).*

model that fits the data. The smoothest model, by definition, is one that contains the minimum amount of structure demanded by the data.

The first step in geophysical ERT inversion is to discretize the subsurface resistivity distribution.  To this end, a 3-D regular grid of rectangular prisms (or triangular elements in 2-D) is constructed, each prism being assigned a distinct, uniform resistivity.  The regular prisms are connected by nodes, such that the prisms and their connecting nodes constitute the computational mesh.  The forward algorithm is based upon solving the governing equations (Ohm's law, plus conservation of charge) on this computational mesh (e.g. Wanamaker *et al.* 1987).  Once the computational mesh is generated, the next step is to parameterize the subsurface resistivity model.  In order to reduce the complexity of subsurface structure where the measured apparent resistivity does not require it, in our approach the model roughness is minimized.  A useful measure of subsurface roughness is specified by:

$$R_1 = \| \partial_y m \|^2 + \| \partial_z m \|^2 \tag{3.16}$$

where the first term on the right-side describes the roughness of the resistivity contrasts in laterally adjacent prisms, while the second term describes the roughness of the resistivity contrasts in vertically adjacent prisms.  The model parameters, i.e. the prism resistivity values, are assembled into the vector $m$.  A smooth inversion based on minimizing $R_1$ is referred to as "first derivative smoothing". In a smooth model inversion, the misfit of the smooth-model response to the data is quantified by the L2 error norm $X^2$, given by:

$$X^2 = \| Wd - WF[m] \|^2 \tag{3.17}$$

where $d$ is the data vector comprising the measured apparent resistivities. The equations

that contain the physics of the forward problem are represented by the nonlinear

functional $F[m]$, with $m$ being the vector of resistivity prism values (i.e. model

parameters), while $W$ represents the data covariance matrix. It is assumed that the noise

is Gaussian and uncorrelated, so that $W$ is a diagonal matrix and, if the diagonal

elements are appropriately normalized, this results in the L2 error measure $X^2$ being chi-

squared distributed with an expected value equal to M, the length of the data vector. In

order to minimize the roughness measure $R_1$, while keeping the error between the

calculated and observed responses at or close to its expected value, an unconstrained

optimization problem must be formulated.

This is easily completed using the classical Lagrange multiplier approach. As the

key step in developing an iterative inversion algorithm, the nonlinear unconstrained

functional $U(m)$ is built as:

$$U[m] = \| \partial_y m \|^2 + \| \partial_z m \|^2 + \mu^{-1}\{\| Wd - WF[m] \|^2 - X^2\} \tag{3.18}$$

with $U[m]$ representing the unconstrained functional to be minimized and the Lagrange

multiplier is written as $\mu^{-1}$. Minimization of $U(m)$ is attained when the vector gradient

of the pair $(m, \mu^{-1})$ equals zero. To linearize equation (3.18), a Taylor expansion is

used to give the following approximation of $F[m]$:

$$F[m_i + \Delta] = F[m_i] + J_i(\Delta) \tag{3.19}$$

$$\Delta = m_{i+1} - m_i \tag{3.20}$$

with $J_i$ representing the Jacobian matrix of partial derivatives of $F[m]$,

$$J_i = \left(\frac{\partial F}{\partial m}\right)_{m=m_i} \tag{3.21}$$

Substuting equations (3.19-3.21) into equation (3.18) and solving for $m_{i+1}$, the updated

model results in:

$$m_{i+1} = m_i + [\mu(\partial_y^T \partial_y + \partial_z^T \partial_z) + (WJ_i)^T WJ_i]^{-1}(WJ_i)^T Wd \tag{3.22}$$

This expression represents a sequence of updated models. The "best" model is obtained

as the one that first attains the specified level of misfit (DeGroot-Hedlin & Constable

1990). The inversion process for 2D ERT data can thus be formulated in these six steps:

I) create a starting resistivity model according to a sensible rule, such as: the average

apparent resistivity; some other aspect of the apparent resistivity distribution; a user

assumption such as intuition, judgment, or previous experience working at a similar site;

or a priori knowledge from other geophysical information about the subsurface

resistivity distribution; II) produce a predicted response by solving the governing

equations for the starting model using the forward modelling process; III) determine the

misfit of the current model using (3.17) and build the Jacobian matrix (3.21); IV) update

the resistivity model using equation (3.22); V) run the forward modeling algorithm using

the updated model; VI) calculate the new misfit between predicted and measured

responses. Steps III through VI are repeated until model convergence is reached, i.e. the

stopping criterion of the specified misfit level is attained (Loke 1995).

A key step in this process is the selection of an appropriate forward modeling

algorithm (step II). To better understand the forward modelling process, it should be

recalled that the apparent resistivity data are generated by an energization of the Earth

through the injection and withdrawal of current using a point source/sink pair, which are achieved using finite-sized electrodes that are represented as three-dimensional objects.

The subsurface resistivity distribution, on the other hand, is defined only in two dimensions, i.e. the vertical plane containing the electrode array. This geometry (a 3-D source energizing a 2-D model) is sometimes referred to 2.5-dimensional. To illustrate the 2.5D ERT forward problem mathematically, the governing equations are expressed by the following 2D partial differential equation in the Fourier along-strike ($y$-direction) wavenumber domain:

$$\frac{\partial}{\partial x}\left(\sigma \frac{\partial V}{\partial x}\right) + \frac{\partial}{\partial z}\left(\sigma \frac{\partial V}{\partial z}\right) - k^2 \sigma V = -I \cdot \delta(x) \cdot \delta(z) \tag{3.23}$$

where $V(x, k, z)$ is the scalar electrical potential in the wavenumber domain, and I is the electric current of the source. The electrical conductivity, reciprocal of resistivity, is represented by $\sigma(x, z)$, while k is the along-strike wavenumber.

The finite element method with rectangular elements, as described above, is used to solve equation (3.23). For each choice of wave number k, the discretization of (3.23), and specification of the relevant boundary conditions, leads to a system of linear equations (AGI 2009). The linear system of equations is then solved using the Cholesky decomposition method. Once the linear system is solved for a range of wavenumber values, the final step in the forward modelling process is to transform the potentials from the wavenumber domain back into the spatial domain (Degroot-Hedlin & Constable 1990). This is easily achieved using an inverse Fourier transform.

RESULTS

Results from the ERT inversions show varying zones of resistivity along the downslope transects B2 and B4 (Figure 3.9 and 3.10), while the along-slope transects B5 and B6 (Figure 3.11 and 3.12) show larger, more consistent resistivity zones. Figure 3.13 - 3.16 show crossplots of measured vs. predicted apparent resistivity values, while Figure 3.17 - 3.20 show the convergence curve for each transect for the first fifteen (15) iterations. It is pragmatic not to underestimate or overestimate an acceptable level of misfit if no prior knowledge about the subsurface is specified. Therefore, fifteen iterations were chosen to generate an intermediate fit of the forward response to the measured apparent resistivity.

Transect B2 (Figure 3.9) reached an imaging depth of ~25 m. Beginning at the top of the slope, a highly resistive zone (~ 1000 ohm-m) is found near the crest of the eroded hogback. At shallow depths down the slope, small areas of highly resistive zones (~ 500 – 1000 ohm-m) surrounded by intermediate resistive zones (~ 100 ohm-m) are present. The slope toe (~ 60 – 100 m from starting electrode) shows indications of low resistivity (~10-30 ohm-m). Results from the inversion show that the model converged (Figure 3.17) before the fifteenth iteration with a RMS (root mean square) error of 9.34%. The crossplot (Figure 3.13) shows good correlation between the measured and predicted apparent resistivity values.
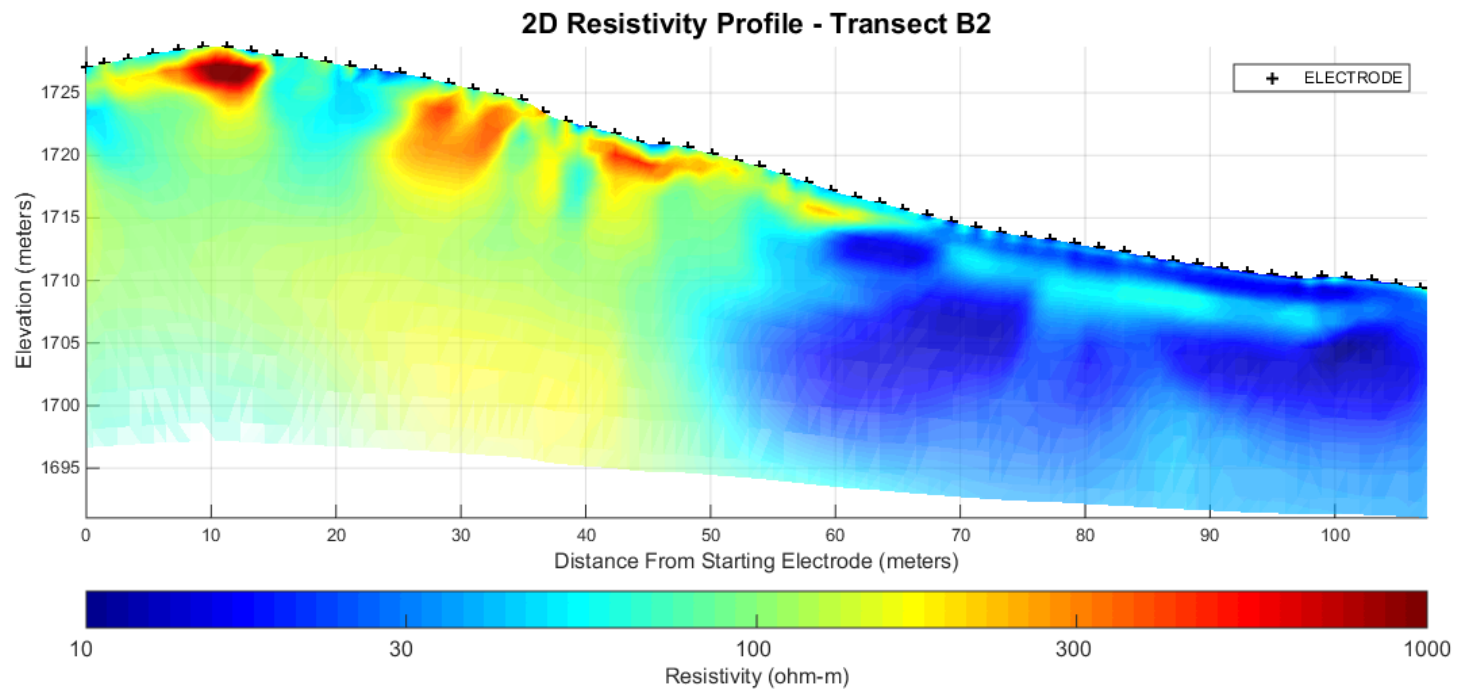
*Figure 3.9: Transect B2 smooth model inversion using fifteen (15) iterations with an electrode spacing set at 2 meters.*
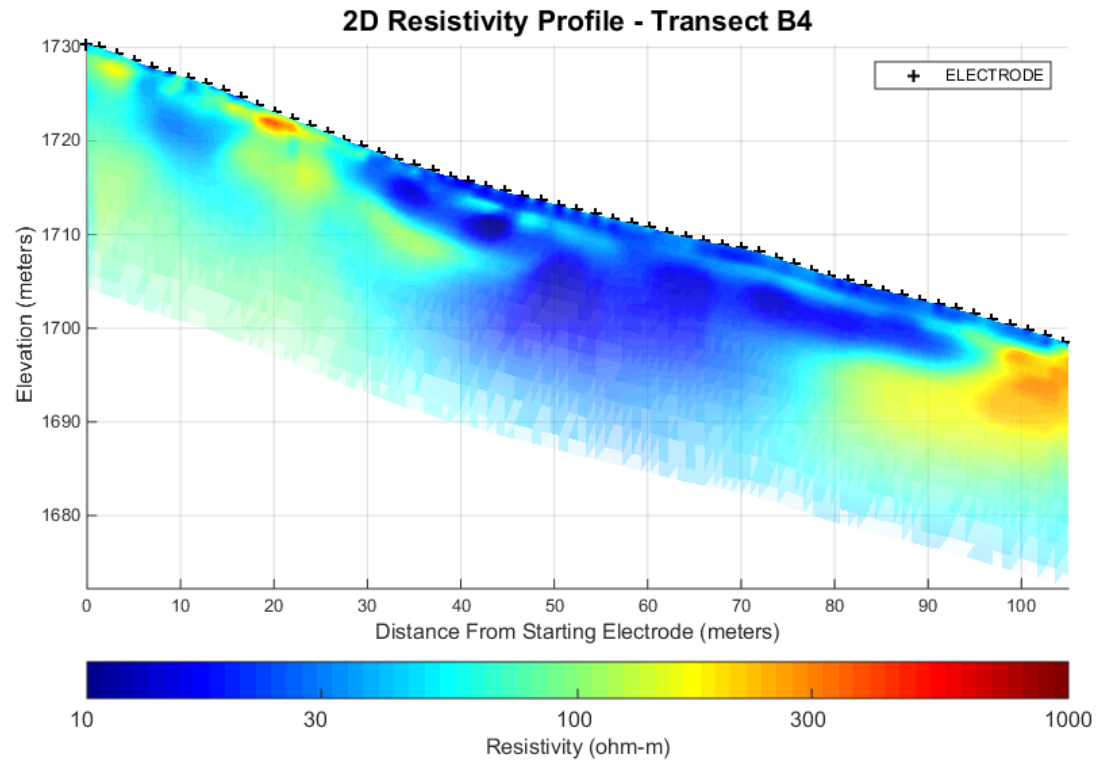
*Figure 3.10: Transect B4 smooth model inversion using fifteen (15) iterations with an electrode spacing set at 2 meters.*
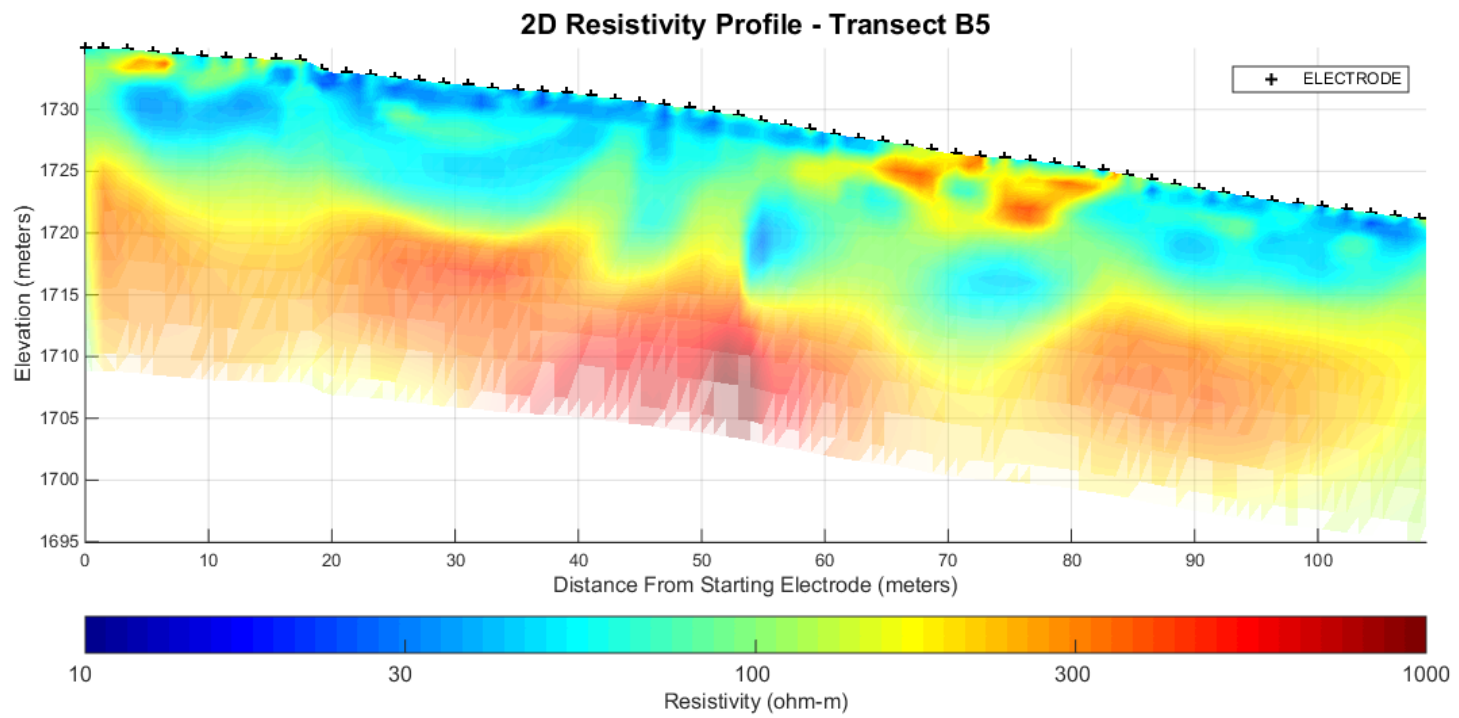
*Figure 3.11: B5 smooth model inversion using fifteen (15) iterations with an electrode spacing set at 2 meters.*
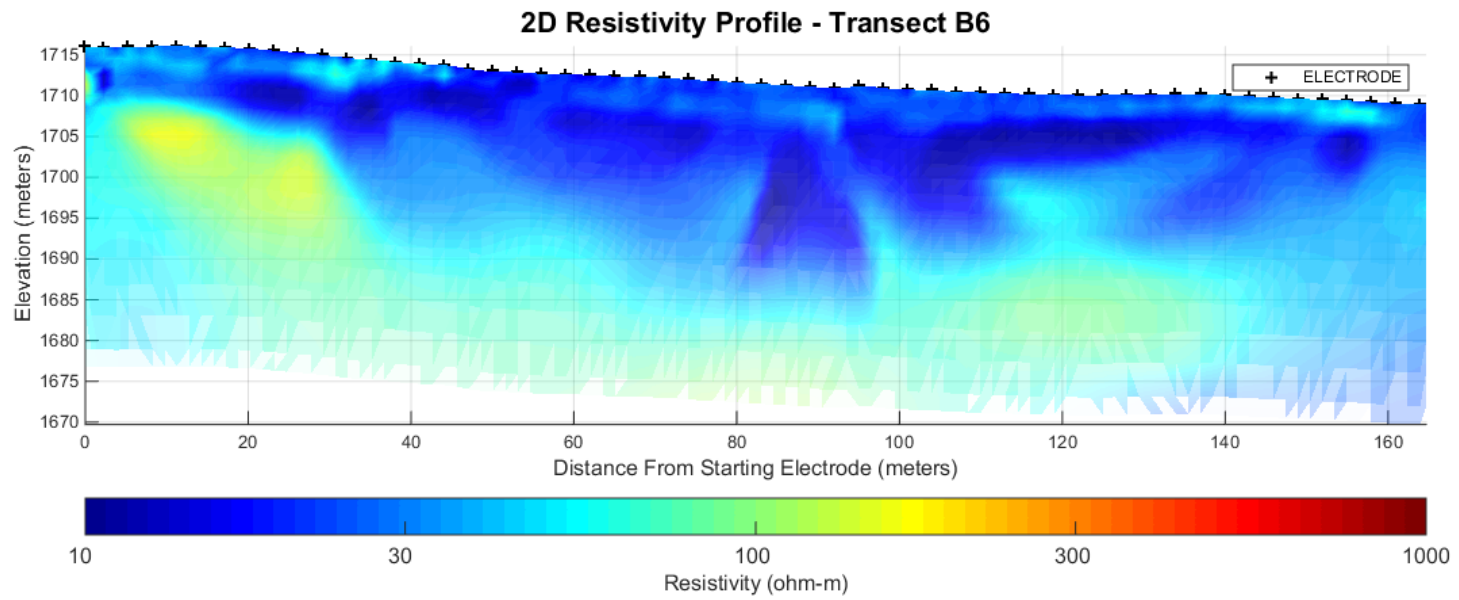
*Figure 3.12: Transect B6 smooth model inversion using fifteen (15) iterations with an electrode spacing set at 2 meters.*
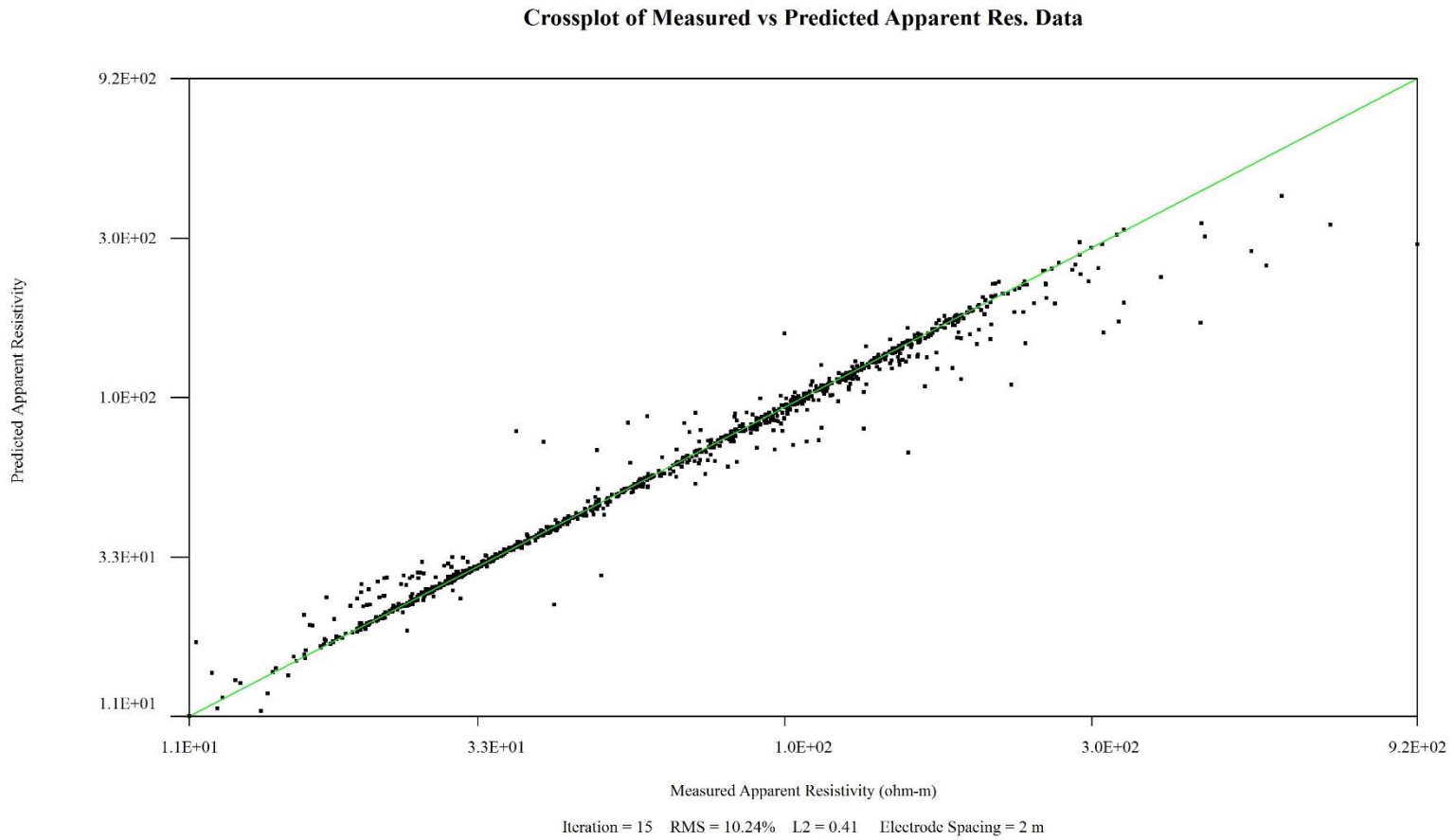
*Figure 3.13: Crossplot of measured vs. predicted apparent resistivity values for transect B2 after fifteen (15) iterations.*

**Crossplot of Measured vs Predicted Apparent Res. Data**



Iteration = 15    RMS = 12.73%    L2 = 0.54    Electrode Spacing = 2 m
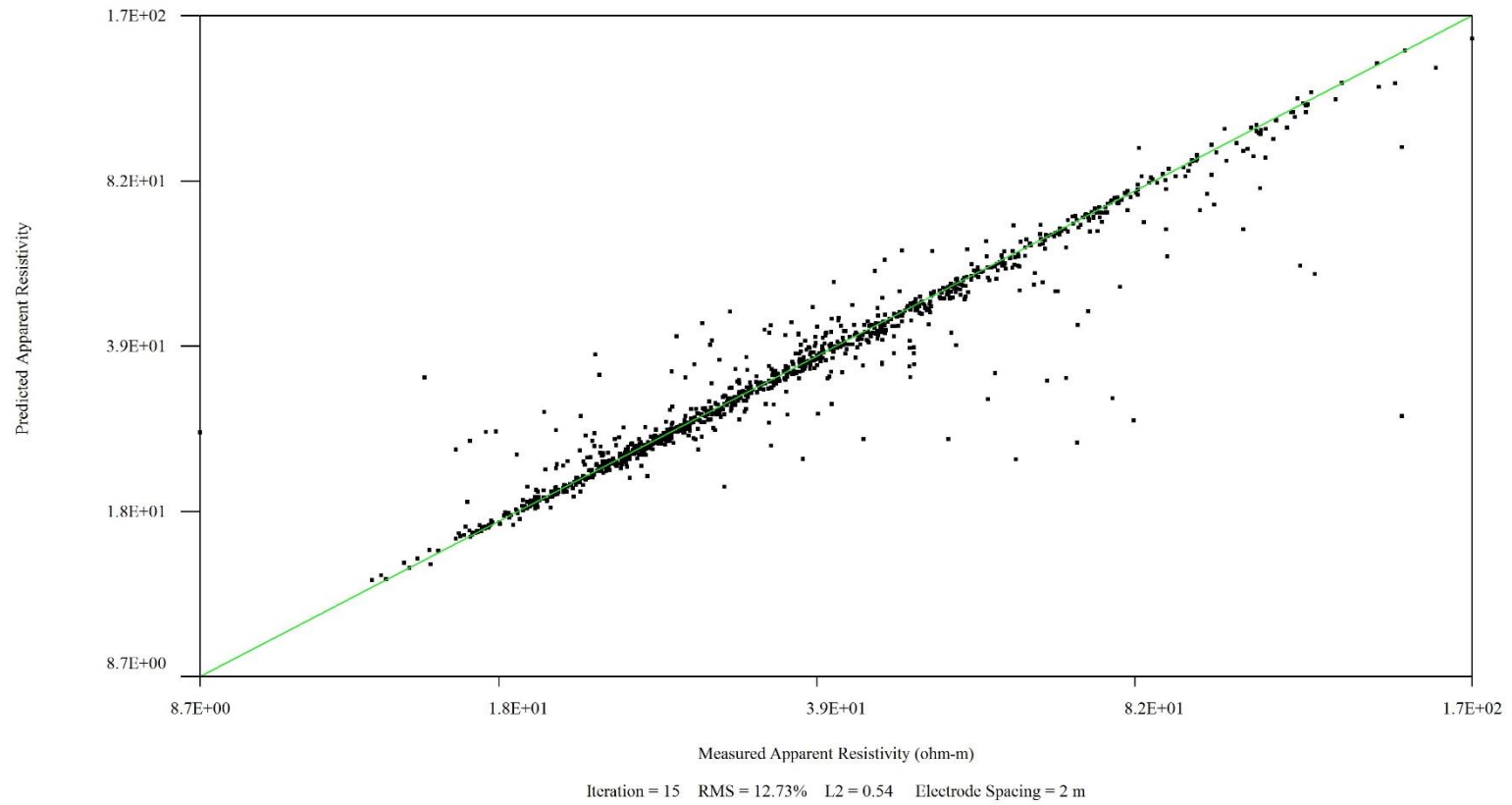
*Figure 3.14: Crossplot of measured vs. predicted apparent resistivity values for transect B4 after fifteen (15) iterations.*

**Crossplot of Measured vs Predicted Apparent Res. Data**
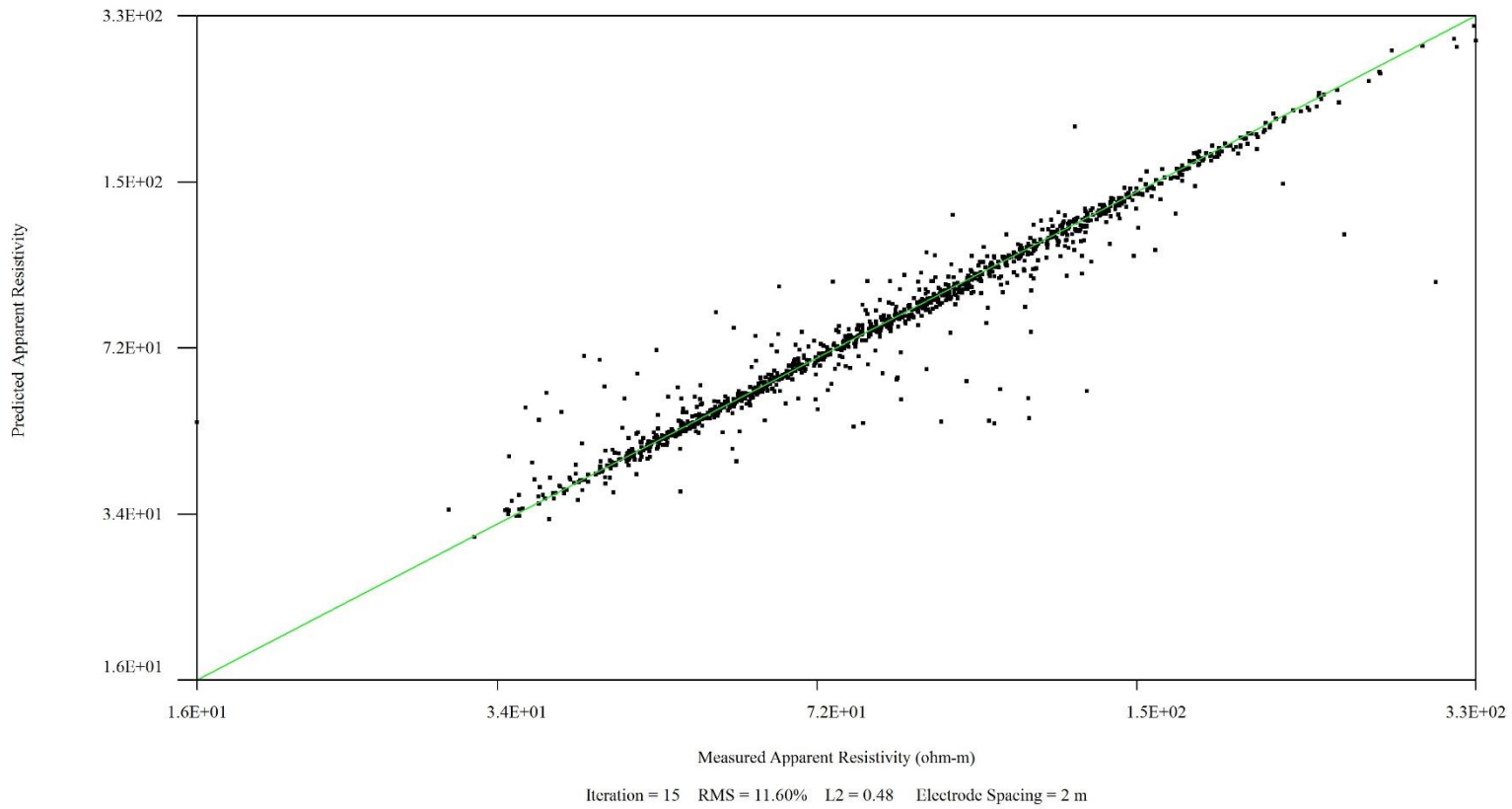
*Figure 3.15: Crossplot of measured vs. predicted apparent resistivity values for transect B5 after fifteen (15) iterations.*

**Crossplot of Measured vs Predicted Apparent Res. Data**

Iteration = 15     RMS = 12.03%     L2 = 0.36     Electrode Spacing = 3 m
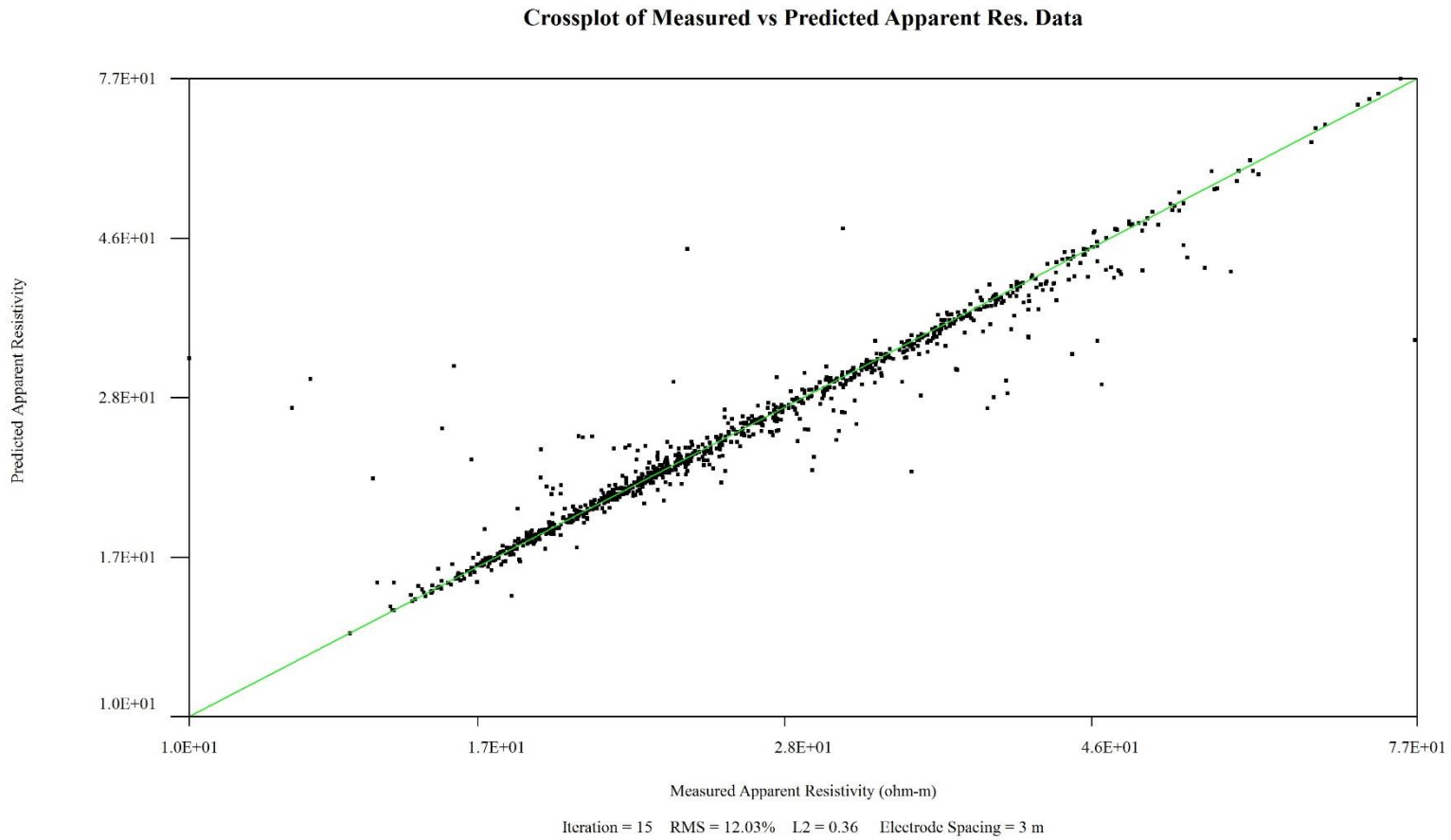
*Figure 3.16: Crossplot of measured vs. predicted apparent resistivity values for transect B6 after fifteen (15) iterations.*

**Convergence Curve of Resistivity Inversion**
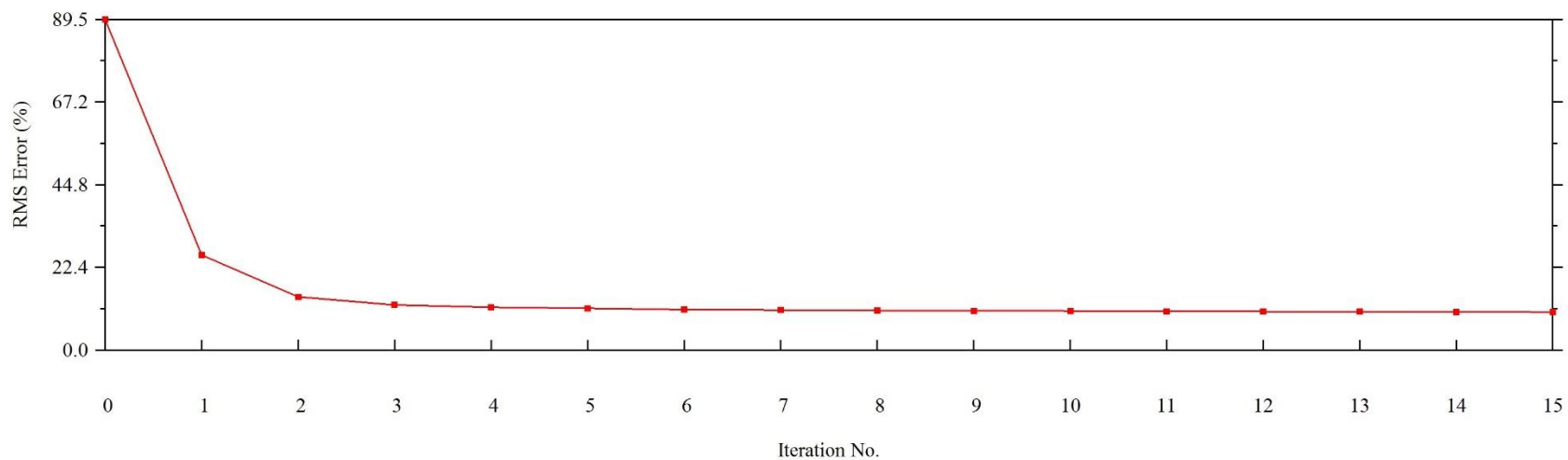


*Figure 3.17: Convergence curve showing predicted model convergence to measured apparent resistivity through fifteen (15) iterations for transect B2.*

*Figure 3.18: Convergence curve showing predicted model convergence to measured apparent resistivity through fifteen (15) iterations for transect B4.*

**Convergence Curve of Resistivity Inversion**
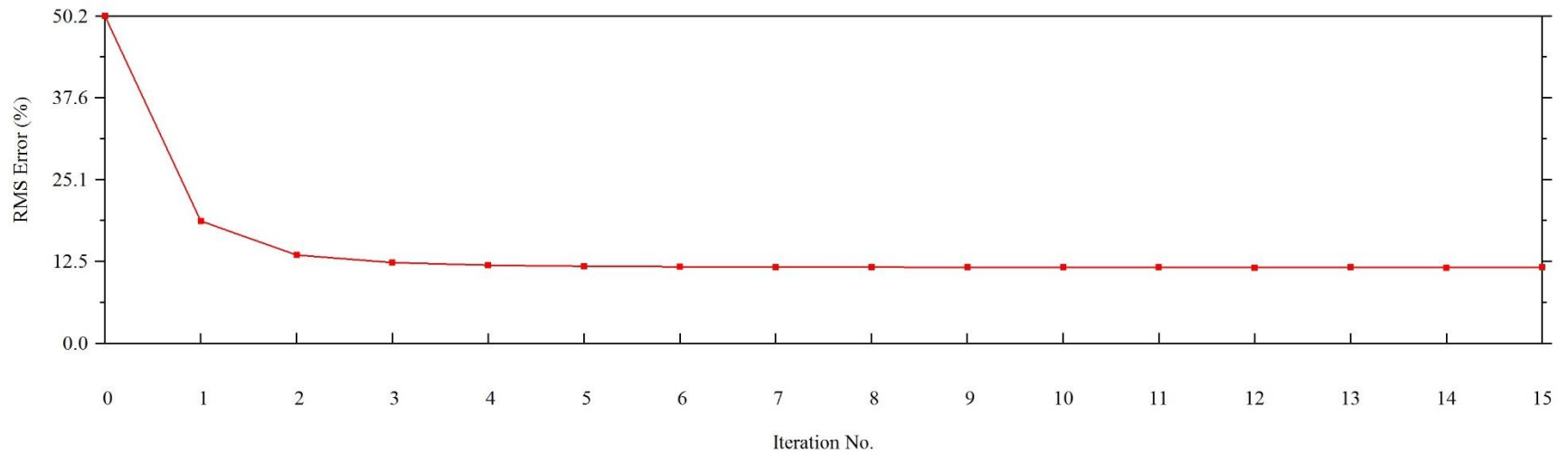
*Figure 3.19: Convergence curve showing predicted model convergence to measured apparent resistivity through fifteen (15) iterations for transect B5.*

**Convergence Curve of Resistivity Inversion**
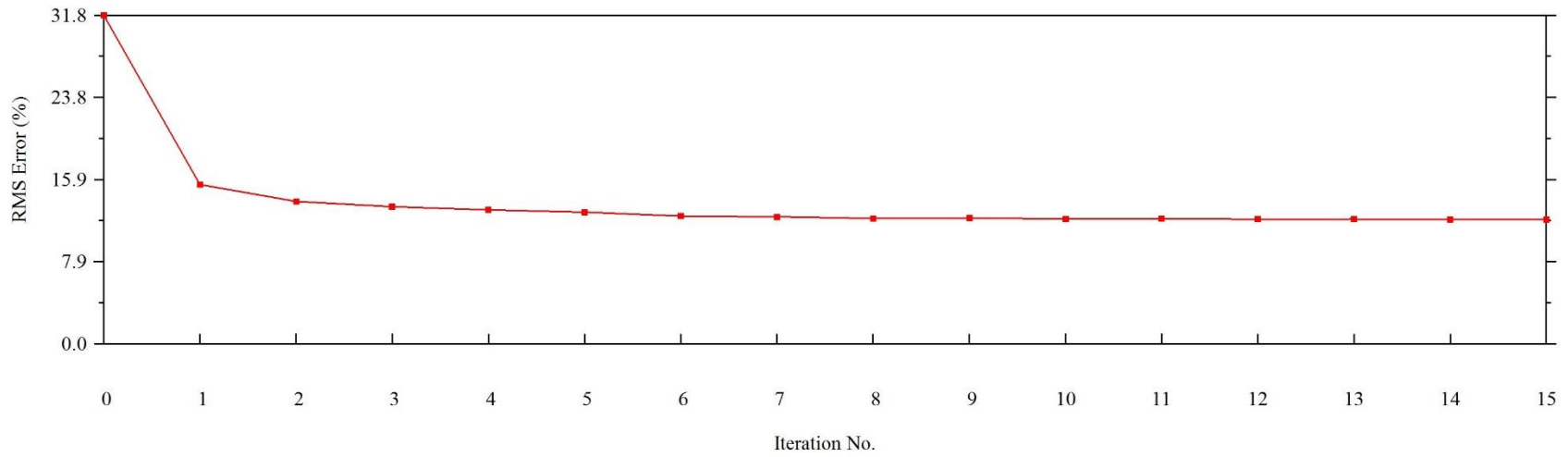
*Figure 3.20: Convergence curve showing predicted model convergence to measured apparent resistivity through fifteen (15) iterations for transect B6.*

Transect B4 (Figure 3.10) shows relatively high resistivity zones (~100-300 ohm-m) further upslope while mid-slope (~ 30 – 90 m in the $x$-direction) shows lower resistivity.  There are two pockets of high resistivity (~ 300 – 1000) on the upper mid-slope at shallow depth (~ 1- 4 m), and at the toe of the slope (~ 100 m).  Inversion results show convergence (Figure 3.18) before the fifteenth iteration (similar to transect B2) with a RMS error of 12.94 %.  Measured vs. predicted apparent resistivity values (Figure 3.14) are less correlated than those at transect B2.

Transect B5 (Figure 3.11) shows highly resistive zones (~ 300 – 1000 ohm-m) along the lower half of the profile.  Less resistive zones are prevalent along the upper half (less than ~ 10 m depth) of the profile. There is a high resistive zone ~ 70 – 80 m from starting electrode to a depth no more than ~ 10 m depth.  The RMS error reached 11.92% (Figure 3.15) with the measured vs. predicted apparent resistivity correlation similar to that of transect B4 and less correlated than that of transect B2.  Convergence occurred before the fifteenth iteration (Figure 3.19).

Transect B6 (Figure 3.12) shows low resistive zones (~ 10 – 30 ohm-m) along the upper half of the profile, while the lower half shows a consistently intermediate resistive zone (~ 100 ohm-m). The RMS error reached 12.40% (Figure 3.20) and again convergence occurred before the fifteenth iteration.  The correlation between the measured and predicted apparent resistivity values (Figure 3.16) is similar to those of transects B4 and B5.

## 4. ERT DATA ANALYSIS, INTERPRETATION AND DISCUSSION

DATA ANALYSIS AND INTEPRETATION

Inversion of ERT data into a two – dimensional resistivity image achieves the transformation of raw scientific data into more easily understood information about the subsurface.  The inversion results comprise a resistivity model that can potentially outline approximate zones of unconsolidated and consolidated soil-rock subsurface, indicating changes in lithology that can govern the groundwater flow characteristics.  In some such cases, a scenario exists in which hydraulic conductivities (the soil's ability to transmit pore fluids) are not large enough to prevent a debris flow slip surface from forming (Lee *et al.* 2012).  In particular, during an intense rainfall event, hydraulic conductivity may not be adequate to prevent a pore pressure increase (Johnson and Sitar 1990). The excess pore pressure destabilizes the soil if the reduced shear-resisting force is overcome by gravitational driving force (Iverson 1997).

Reid and Iverson (1992) simulated how hydraulic conductivity heterogeneities can impact groundwater flow paths, which in turn influence slope stability during rainfall events.  This can be seen in Figure 4.9 where, depending on the hydraulic conductivity value, the pore pressure (hydraulic head) can either increase or decrease.  In terms of geomorphology along the slopes in Boulder, Colorado, the interaction between heterogeneous subsurface soil-rock interfaces is expected to contribute to a loss of shear-resisting force during rainfall events.

To better recognize potential debris flow slip surface areas within ERT maps, a spatial resistance change (SRC) parameter is defined as:

$$\Delta\rho = \sqrt{\left(\frac{\partial\rho}{\partial x}\right)^2 + \left(\frac{\partial\rho}{\partial z}\right)^2} \qquad (4.1)$$

where $\Delta\rho$ is the change in spatial resistivity, $\rho$ is the resistivity and $x,\ z$ are spatial coordinates of the ERT maps. Once the data were inverted using AGI Earthimager software, the resistivity distribution of the final model was uploaded into MATLAB® and analyzed according to the above equation (4.1) (see Appendix for code). The resulting SRC map shows the change in resistivity with units of ohm-m/m. Ultimately, this generates a 2-D resistivity profile showing areas where a spatial change in lithology is present. Such areas may indicate subsurface features associated with debris flows.

Figure 4.2– 4.4 shows the results of implementing this algorithm on the ERT transects acquired for this study. Each transect was compared to a maximum allowed change in resistivity (ohm-m/m), seen in the subplots of Figure 4.2– 4.8. The chosen maximum allowed change in resistivity for image purposes was 100 ohm-m/m for transects B2-B5, and 50 ohm-m/m for transect B6. This highlighted complex geomorphologic areas while still remaining conservative to changing soil/rock compositing and acquisition noise.
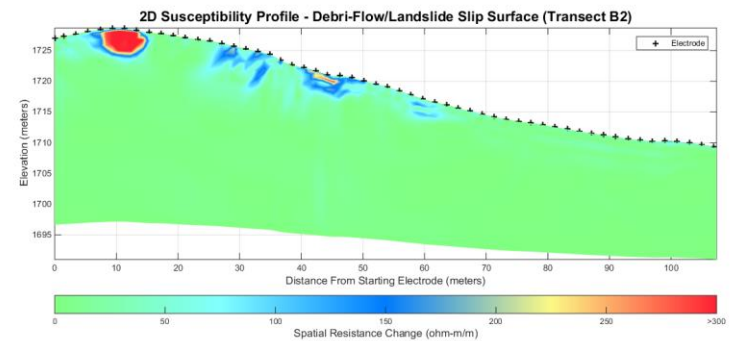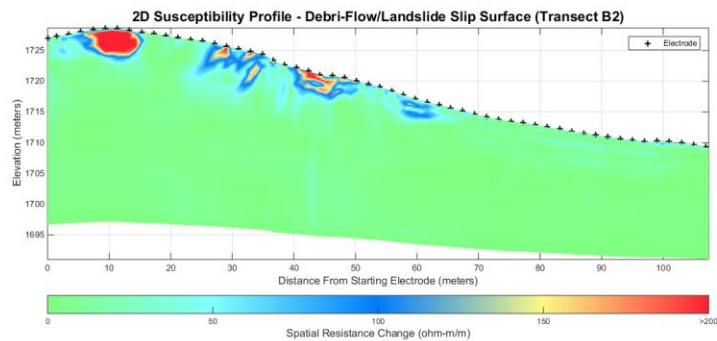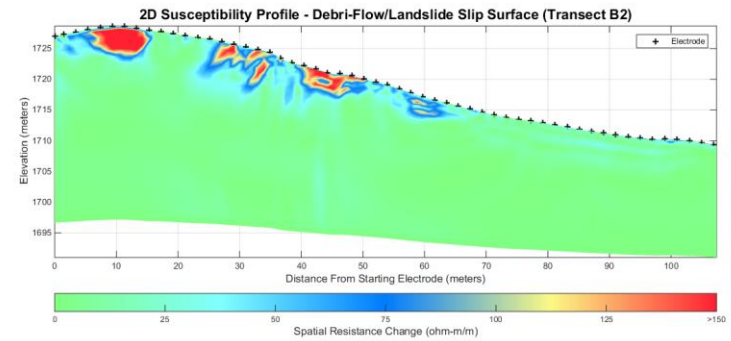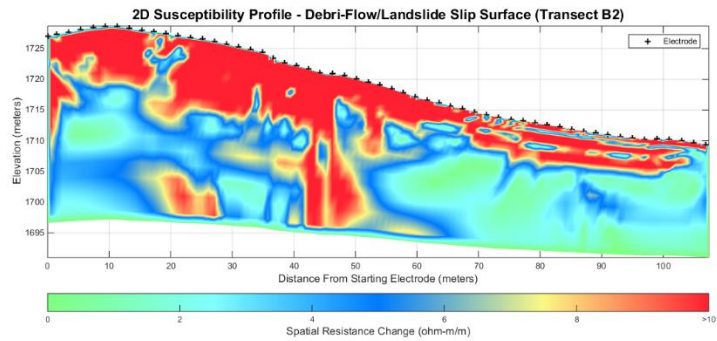
*Figure 4.1: Spatial resistance change maps for Transect B2 showing areas where the change in spatial resistivity is present within the inverted ERT map. **Top left** – maximum change is 10 ohm-m/m; **Top right** – maximum change is 100 ohm-m/m; **Bottom left** – maximum change is 200 ohm-m/m; **Bottom right** – maximum change is 300 ohm-m/m.*
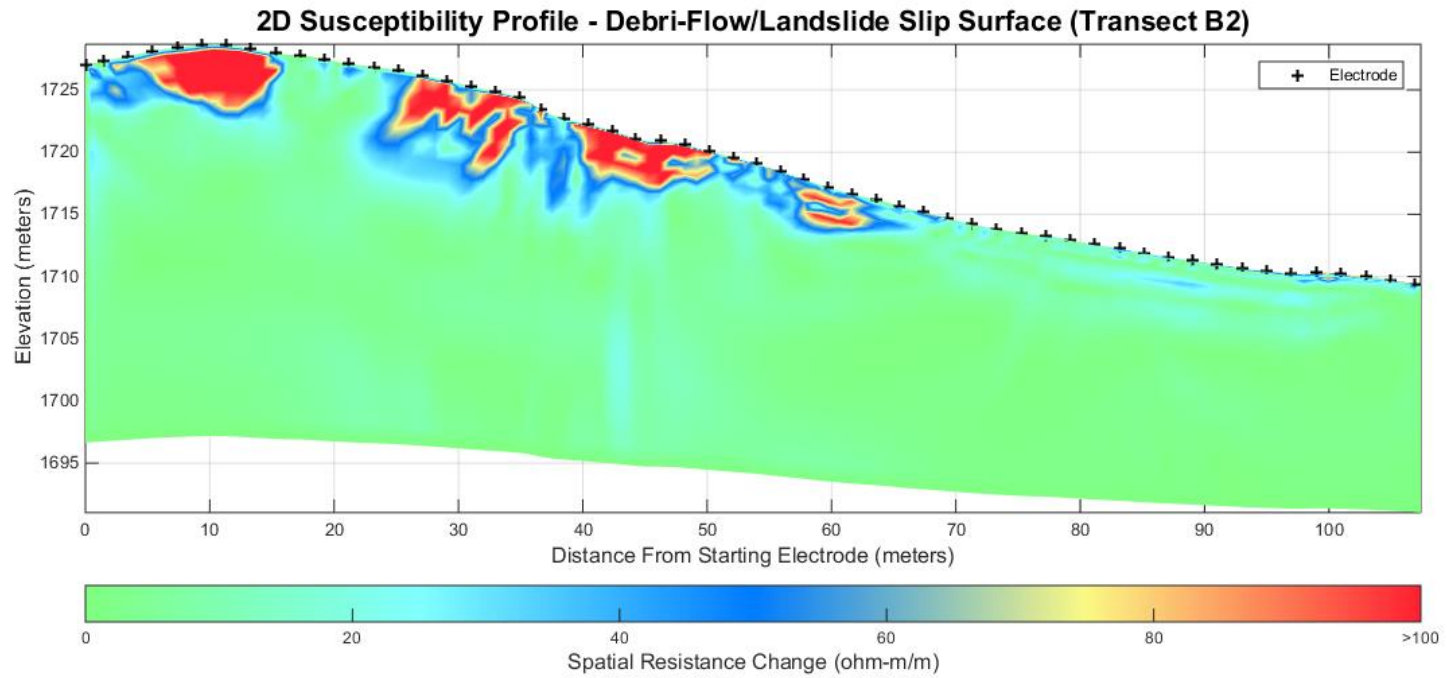
*Figure 4.2: Spatial resistance change map for Transect B2 showing areas where the change in spatial resistivity is present within the inverted ERT map – maximum change of 100 ohm-m/m.*
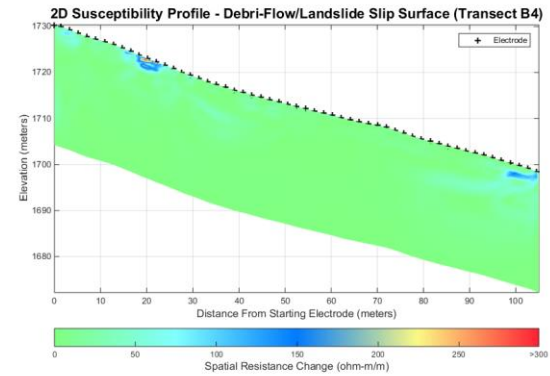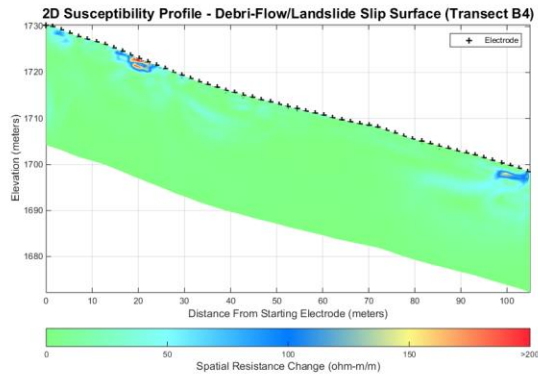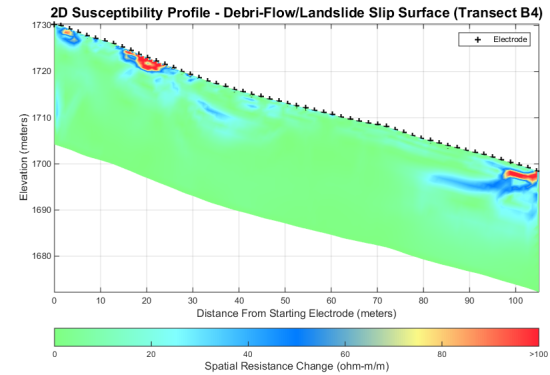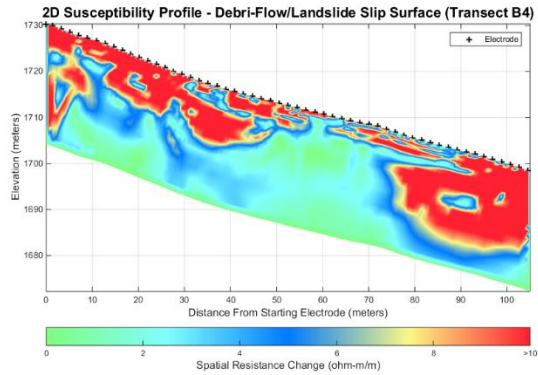
*Figure 4.3: Spatial resistance change maps for Transect B4 showing areas where the change in spatial resistivity is present within the inverted ERT map.* **Top left** *– maximum change is 10 ohm-m/m;* **Top right** *– maximum change is 100 ohm-m/m;* **Bottom left** *– maximum change is 200 ohm-m/m.*
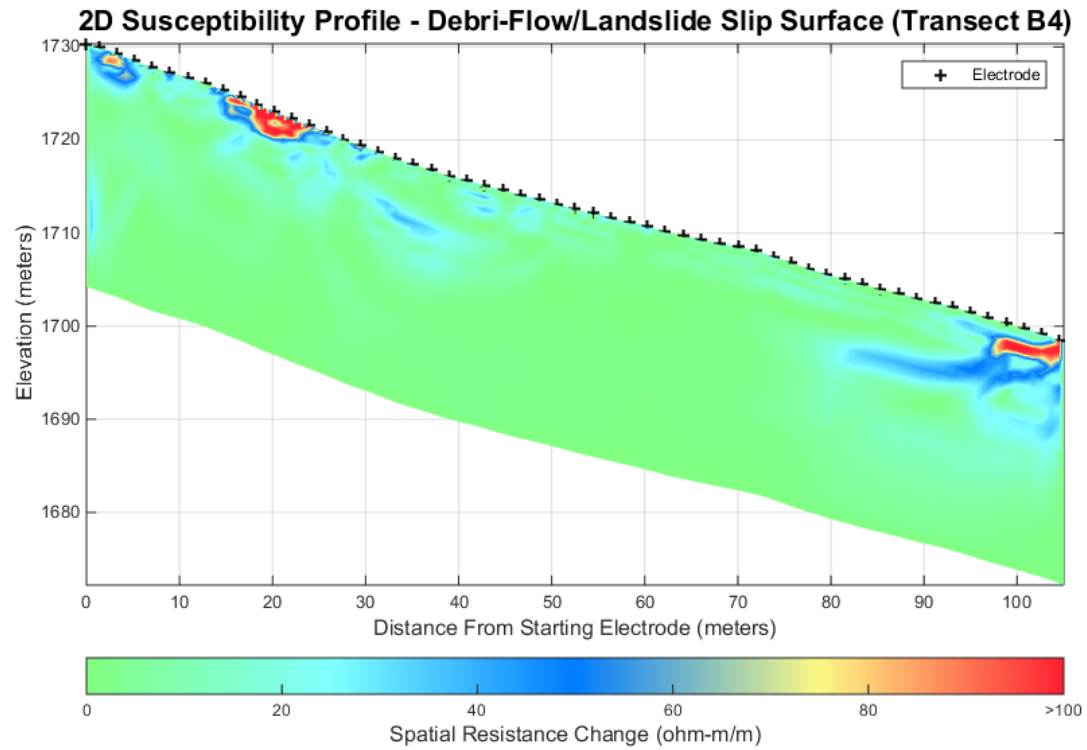
*Figure 4.4: Spatial resistance change map for Transect B4 showing areas where the change in spatial resistivity is present within the inverted ERT map – maximum change of 100 ohm-m/m.*
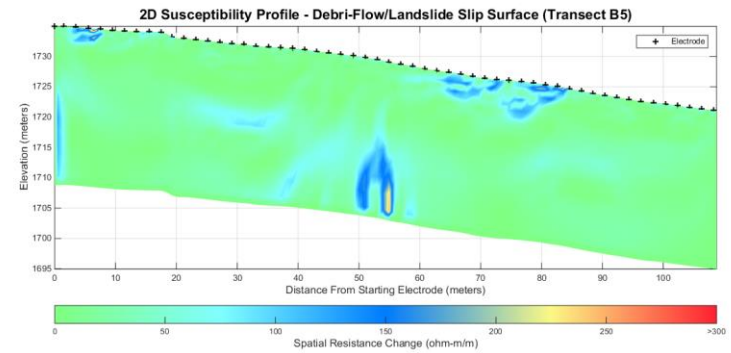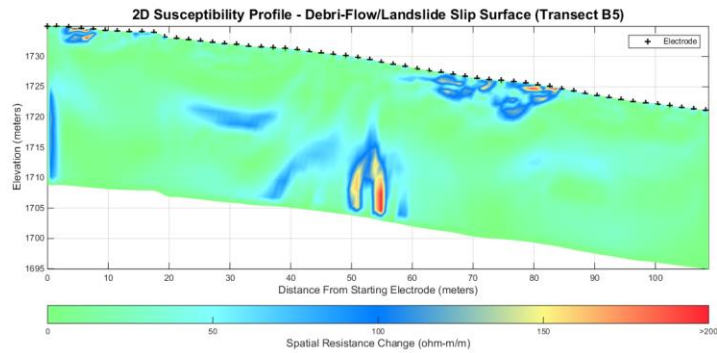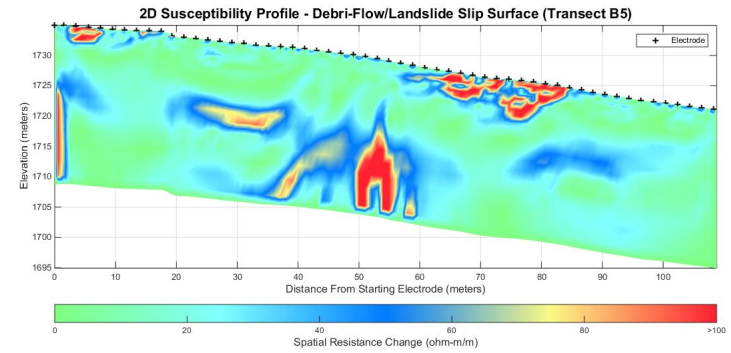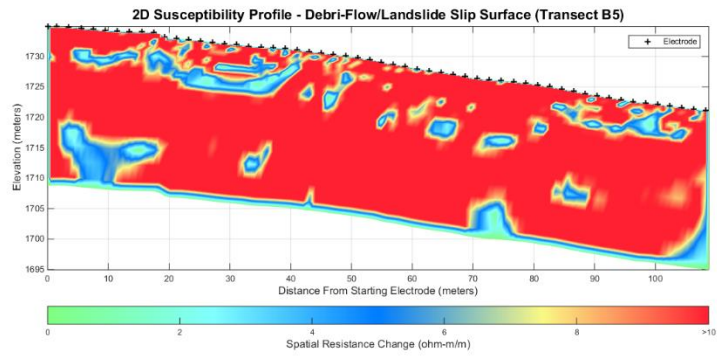
*Figure 4.5: Spatial resistance change maps for Transect B5 showing areas where the change in spatial resistivity is present within the inverted ERT map. **Top left** – maximum change is 10 ohm-m/m; **Top right** – maximum change is 100 ohm-m/m; **Bottom left** – maximum change is 200 ohm-m/m.*

53
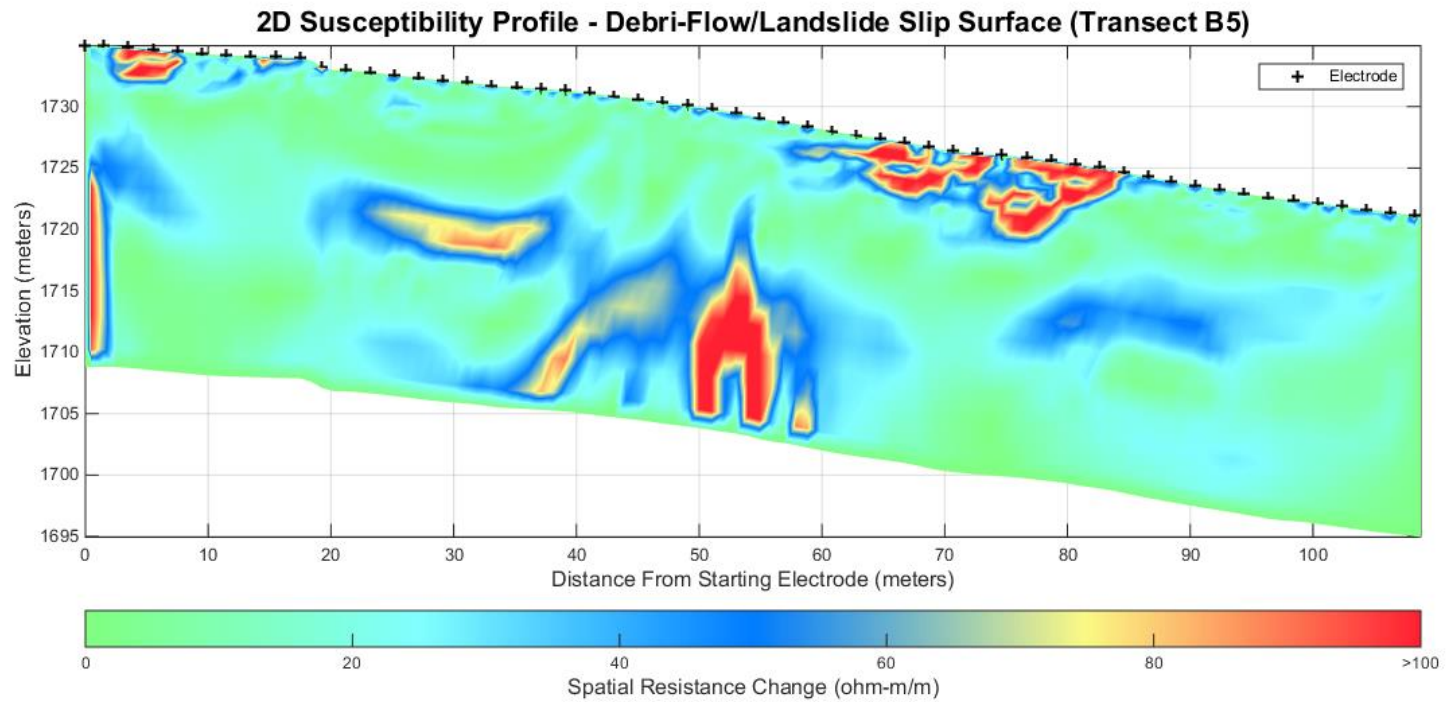
*Figure 4.6: Spatial resistance change map for Transect B5 showing areas where the change in spatial resistivity is present within the inverted ERT map – maximum change of 100 ohm-m/m.*
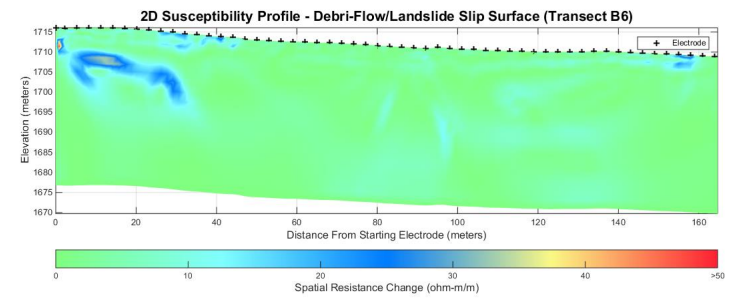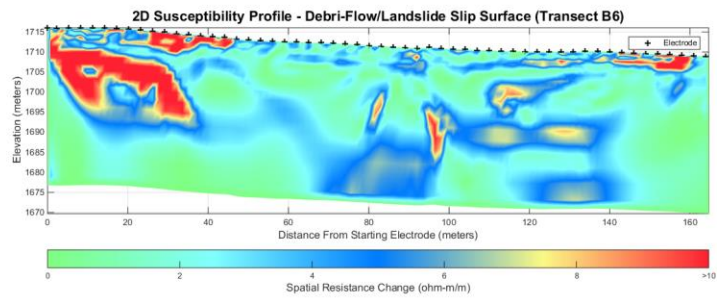
*Figure 4.7: Spatial resistance change maps for Transect B6 showing areas where the change in spatial resistivity is present within the inverted ERT map.* **Top left** *– maximum change is 10 ohm-m/m;* **Top right** *– maximum change is 50 ohm-m/m.*
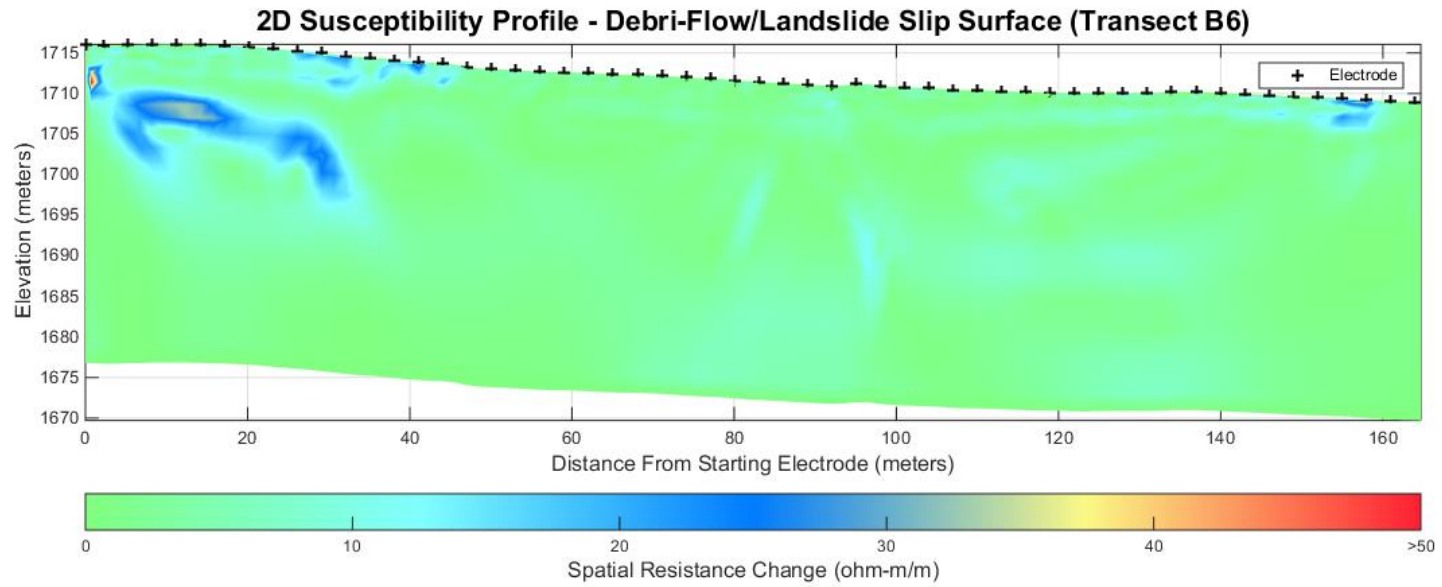
*Figure 4.8: Spatial resistance change map for Transect B6 showing areas where the change in spatial resistivity is present within the inverted ERT map – maximum change of 50 ohm-m/m.*
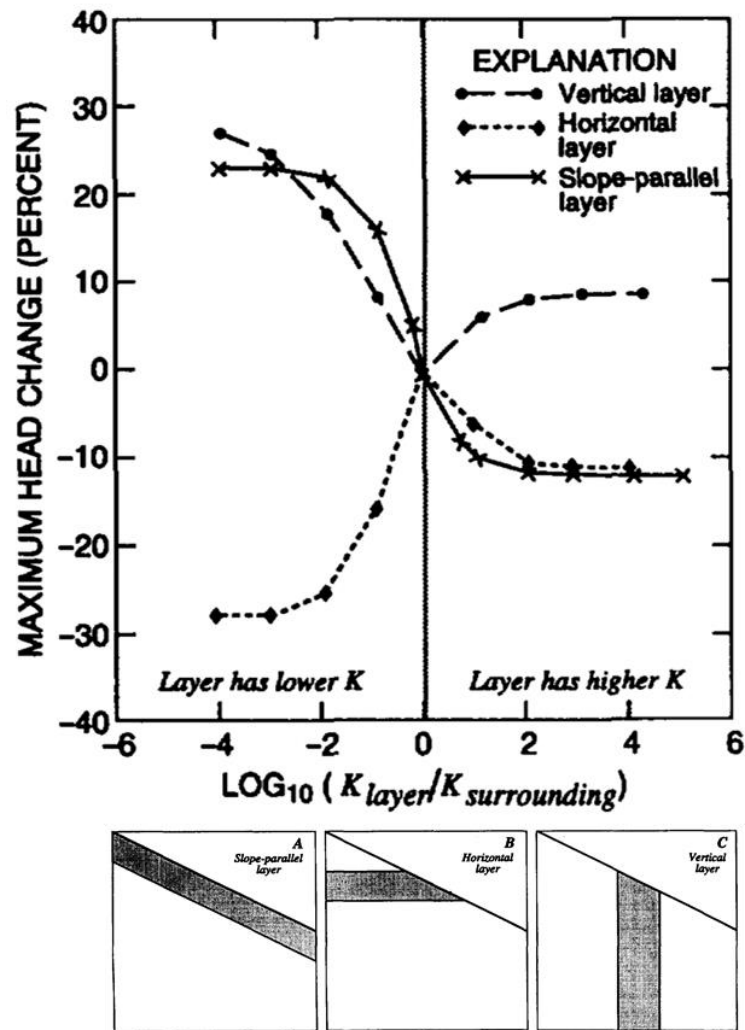
*Figure 4.9: Model response of hydraulic head (pore pressure) as a result of interaction between varying hydraulic conductivity (K) with different lithologic orientations (Reid & Iverson 1992).*

Data acquisition occurred during a relatively dry period through the dates of

March 27 -30, 2015 (there was 9.7 mm total rainfall for the month of March 2015).  The

low amount of rainfall led to the assumption that much of the ground water was drained

and approaching steady-state following recovery from the last precipitation event. Under these conditions, low resistivity zones (10-30 ohm-m) are interpreted as colluvium consisting predominately of clay. Areas where the resistivity is high (200-1000 ohm-m) are assumed to be bedrock, and intermediate resistivity zones (50-200 ohm-m) are interpreted as colluvium consisting predominately of sand/gravel (Table 1).

Transect B2 (Figure 4.2) shows large areas of high spatial change in resistivity at ~25 – 65 m along the strike direction (x-axis), reaching a depth of ~10 m. A smaller zone of very high resistance change is located at the crest of the profile (~10 m in the strike direction). The most extensive region of spatial resistance change is located at mid-slope. This is likely indicative of an area where a complex hydrogeological structure exists. The large spatial resistance change at the crest, near the eroded hogback, is probably caused by eroded cobbles, rocks and boulders.

A small area of high spatial resistance change can be seen along transect B4 (Figure 4.4) at ~20 m along strike and ~5 m depth. This area may be correlated with Transect B2 where the complex hydrogeological structure is present. An area at the toe of the slope (~100 m along strike) shows spatial resistance change that could be interpreted as caused by larger colluvium clasts. These could reside in a buried erosional gully or be remnants from the historic landslide seen in Figure 3.4. Transect B5 (Figure 4.6) shows a resistance change ~ 60-80 m in the $x$-direction with a depth reaching ~ 10 m. This is representative of the crest of the eroded Dakota hogback, as seen in Transect B2. At ~ 15-30 m depth along the profile, a moderate amount of spatial resistance change is seen, which is the interface between colluvium and bedrock. Transect B6

(Figure 4.8) shows no major anomalies in the spatial resistance change parameter.  This lack of a signal is interpreted as a relatively conductive zone consisting of a uniform distribution of soils/rocks.

# 5. RISK PERCEPTION

INTRODUCTION

With rapid habitation in mountainous regions, the need for a cheap and quick method for assessing debris flow susceptibility is essential. ERT has become widely used in debris flow studies for its ability to image complex subsurface geology (Perrone *et al.* 2014). Yet, identification of debris flow susceptible areas is necessary, communicating such hazards to the inhabitants of the area is also critical. Studies have revealed that when critical hazardous information is effectively communicated to the public, the success of a hazardous management plan increases. Steelman (2013) noted when risk communication was utilized before an event, it was associated with the acceptance of a more flexible risk management plan. Essentially, preparation for a hazardous event can ultimately mitigate the loss of life and property.

Geophysical information reveals much about the subsurface regarding risks of natural hazards, yet its inherent ambiguity can lead to confusion and possibly even distrust within the general public. Risk perception is an important field of research in natural hazards and, more generally, resource economics. Essentially, how an individual makes decisions based on his or her exposure to geophysical-based information is of interest to researchers looking for ways to mitigate debris-flow risks (Konishi and Adachi 2011). The term "Risk" is sometimes used to broadly imply that some extent of the probability and severity of an outcome is known. For example, in Boulder County, the risk of another

extreme rainfall event occurring is present and fairly well understood, and hence future debris flow incidence can be assumed. Although these risks seem candid, differences amongst individuals arise with increasing outcome severity. In circumstances which the outcome severity is low with a high occurrence probability as compared to those characterized by a high outcome severity with a low occurrence probability, an individual may perceive and act on these risks with entirely different behaviors (Kunreuther *et al.* 2001). In the present case, the rainfall induced debris flow event in Boulder, Colorado during September, 2013, can be classified as low occurrence probability with a high outcome severity.

An individual making a risk decision based on his or her own prior knowledge, which may not align with geophysical-based predictions, makes references to subjective probabilities (Shaw in press). Subjective probabilities play an important role in societal decision making. This affects the perceptions of health, natural hazards and other risks (Shaw in press). Though subjective probabilities may not have a major impact on day-to-day activities, how an individual perceives risk becomes important to his or her survival. Recognition of the subjective nature of risk-based decisions has led to a better understanding of how individuals update prior knowledge of risks for events which the outcome is life or death. Viscusi (1993) performed multiple studies on this topic, explaining his results within a framework of rational learning. Independent information was introduced to individuals, with or without a priori knowledge, and their responses were evaluated based on which information source most contributed to the updating process. Similarly, Cameron (2005) designed a study about climate change and public risk

perception in which individuals are introduced to uncertain science (i.e., poorly known probabilities). Her study concluded that individuals tend to update their prior knowledge by such mechanisms as Bayesian updating and weighted averages. She also noted that uncertainty or bias can play an important role when an individual updates his or her prior knowledge. This is revealed in cases characterized by an individual's opinion of the credibility or authority of external sources which, if negative, can lead to a lack of attention paid to the information being presented.

In much of the research to date, a primary goal is a better understanding of how natural hazard risks are perceived and how various sources of information are viewed and processed. Designing surveys to identify subjective probabilities is imperative to understanding their effects on perceived risks (Charness *et al.* 2013). For this project, we will not attempt a comprehensive experimental design, but rather explore the concept in a cursory manner by means of an informal focus group. This is of basic interest since little work has been done on public understanding of geophysical imaging results. In essence, this project elicited information regarding risk perception using geophysical-based information that paralleled, but is of reduced scope to, the study performed by Viscusi (1993) noted above.

SURVEY DESIGN

The risk survey will provide a simple indication of changing risk perceptions as the technical level of information is systematically raised.  To quantify this change, a numerical scale from 0-100 is adopted. The scale represents the subjective probability that a debris flow will occur in this area within the next year. The survey asks individuals to record their perception of the risk, with 0 being "definitely will not occur" and 100 being "certain to occur".  At stage 1, the baseline risk perception is assessed by simply introducing the setting of the survey area and the 2013 Boulder, Colorado, flooding and debris flow event. At stage 2, participants are shown meteorological information, geological and susceptibility information regarding the Colorado Front Range. At stage 3, participants are shown SRC maps highlighting areas of subsurface heterogeneity without information showing how it was calculated. At stage 4, participants are shown the operating principles of the ERT geophysical technique and the ERT images from the geophysical mapping. At stage 5, participants are shown the full mathematical details of the ERT technique, along with a highly technical discussion concerning the uncertainties associated with this imaging method. Besides recording subjective probability, each participant is asked at every stage to identify what particular information, if any, prompted them to change their probability assignment and if the information did not change their probability, why.

A small (*N*=9) group of current Texas A&M graduate students studying geology, geophysics, and natural resource economics under Profs. Everett, Giardino and Shaw were recruited to participate in this study.  The survey was performed in a classroom within the Texas A&M University Geology & Geophysics building (Halbouty, lecture room 104) using a PowerPoint presentation showing the 5 stages of information noted above.  It is important to note the recruits may be more representative of stakeholders than members of the public at large.  The Institutional Review Board (IRB) reviewed and approved this survey to be administered to human subjects (IRB2016-0284D).

RESULTS AND INTERPRETATION

The risk perception survey results (Table 2) show the varying responses of the nine (9) participants, who were students within the graduate programs in Geology and Geophysics as well as Agricultural Economics at Texas A&M.

| Participant | Break 1 | Break 2 | Break 3 | Break 4 | Break 5 |
|---|---|---|---|---|---|
| 1 | 100 | 75-100 | 75-100 | Null | Null |
| 2 | 10 | 10 | 10 | 10 | 10 |
| 3 | 40-50 | 50-55 | 50 | 50 | 50 |
| 4 | 60 | 65 | 75 | 75 | 75 |
| 5 | <5 | <5 | 15 | 15 | 15 |
| 6 | 70 | 75 | 75 | 75 | 75 |
| 7 | >20 | >40 | >40 | >40 | >40 |
| 8 | 50 | 30 | 10 | <1 | <1 |
| 9 | 85 | 95 | 95 | 95 | 98 |

*Table 2: Risk perception survey results for a total of nine (N=9) participants. Values are given in probability of debris flow occurring within one (1) year on a scale of 0-100.*

Figure 5.1 shows the change in subjective probability after each successive break. The probabilities were averaged if a range of values were given (for subjective probability change distribution). After exposure to stage 1 of the presentation, the perceived debris flow risk probabilities of the participants spanned a wide range from <5 to 100. After stage 2, all but one participant (participant 2) changed their perceived risk. After stage 3, participants 1, 2, 6, 7 and 9 did not change their perceived risk.
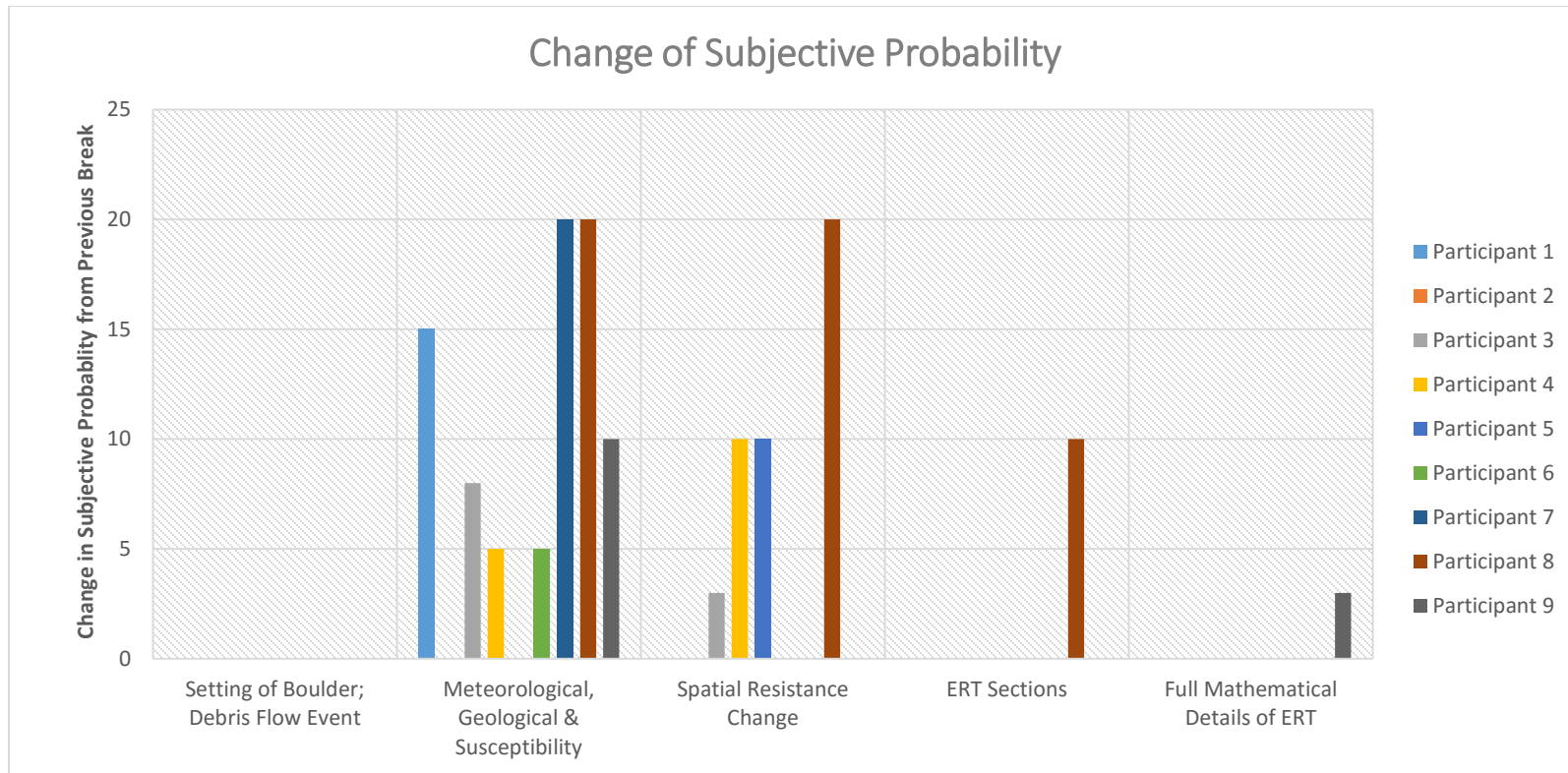
*Figure 5.1: Change in subjective probability from previous break. Break 1 does not show any change due to being the first measure.*

After stage 4, only participants 1 and 8 changing their perceived risk.  After stage 5 at the end of presentation, the perceived debris flow risk of the participants ranged from <1 to 98 with one "null", or "cannot determine".  Participants responded both with both precise values as well as ranges of perceived risk.  Participant 1 responded with "null" after stage 3 of the presentation.

Participants were also asked to give a descriptive justification as to their estimation of probability. Below are the specific set of questions asked during each break in the survey:

- "On a scale of 0-100, what is your perceived probability of a debris flow event occurring within the next year?"

- "What information (if any) directed you to choose this probability?"

- "If your probability did not change based on the information just shown, why?"

The responses from the survey after stages 1 and 2 ranged from individuals who had some prior scientific knowledge of debris flow mechanisms and flood frequency measures, to individuals who have previously lived in debris flow susceptible areas.  These individuals tended to have extreme values for their perceived probability (i.e. <10 to > 90).  Some respondents stated that the photographs showing debris flow destruction led them to choose a certain probability.  The probabilities of these individuals ranged within the median range (i.e. >10 to <90).  Once geophysical information was introduced starting at stage 3 of the presentation, the written responses became more varied.  The written responses ranged from "no new information" was provided by the geophysics, to important

new information was provided by the spatial resistance change maps which indicated areas

debris flow susceptibility (see Appendix for full list of responses).  Some individuals noted

that the geophysical information merely solidified their previous probability assignment.

## 6. CONCLUSIONS

ELECTRICAL RESISTIVITY TOMOGRAPHY

The ERT mapping resulted in four images showing distinct subsurface features typical of highly eroded slopes within mountainous regions. All images show possible areas of colluvium with a probable Dakota Formation provenance. The image from transect B5 (Figure 3.11) shows dominant high resistive (~100-1000 ohm) zones along the $x$-axis at depth ranging from ~ 20-30 m. This is interpreted at bedrock that is striking to the north and dipping to the east. The image from transect B6 (Figure 3.12) shows a similar zone of relatively high resistivity (~100-300 ohm) that is less apparent than that of the B5 image, however it shows similar structure that can be correlated to the bedrock shown in image B5.

Images from transects B2 (Figure 3.9) and B4 (Figure 3.10) show correlating features along mid-slope (~ 20-30 m in the $x$-direction) characterized by a complex resistivity zone. This complexity may indicate an area where the bedrock is close to, or exposed at the surface. It is better seen in the Transect B2 image, where the slope is more eroded relative to the B4 image. This zone is highlighted in the spatial resistance change maps (Figure 4.2- Figure 4.8) and is interpreted as a feature that could be associated with debris flow occurrence. It would be a zone where pore fluid drainage is complex, leading to enhanced debris flow slip surface potential. Further towards the toe of the slope, less resistive (~10 – 50 ohm-m) material is dominant in images B2 and B4 that can be

correlated to Transect B6 along the toe.  The low-resistivity zone is interpreted as either clayey material or a saturated area along the slope.

Figure 6.1 shows a geological interpretation of the slope (at a location closely corresponding to Transect B4, see Figure 3.4) based on the ERT and SRC maps, along with field observations.  Bedrock is expected at depth along the slopes, overlain by a layer of colluvium.  Multiple, highly dipping layers of sedimentary bedrock are expected at depth traversing down slope.  This is inferred from visual observations of the terrain encountered within the Boulder study area, notably the hogbacks and the general unevenness of erosional slopes.  This inference is consistent with the mid-slope areas of the B2 and B4 images, where complex high resistive zones are present along the steep, uneven slope.  The possibility of dipping bedrock below the assumed unconsolidated material may have varying erosional properties, creating a situation where the slope becomes steeper where one bedrock layer doesn't erode as fast as an adjacent layer (i.e. more accommodation space).

Overall, the geophysical mapping showed subsurface geologic indications of the potential cause of the debris flows that occurred along the slopes of Boulder during the September 2013 flooding event.  It is evident that the antecedent rainfall, complex geology, and subsurface hydraulic conductivity are the major controlling factors for the initiation of slip surfaces within the study area, and most probably along greater extents of the Colorado Front Range.  However, in order to better assess the risk of debris flows in Boulder, more geophysical data should be acquired in order to determine a risk level that can be confidently presented to the residents.
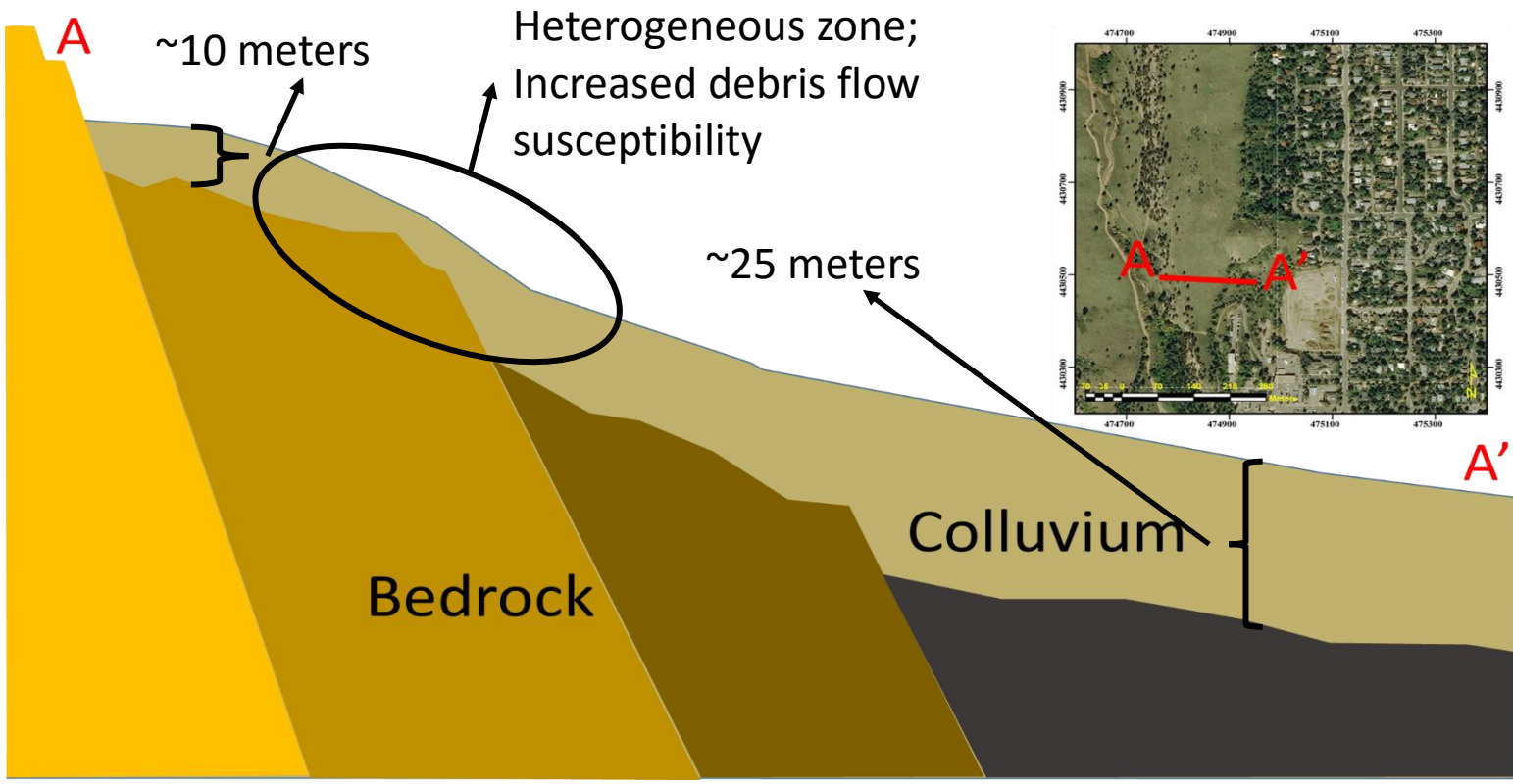
*Figure 6.1: Cross-section depicting subsurface along profile AA' interpreted from ERT data.*

Results from the debris-flow risk perception survey provided interesting results. It was originally expected that individuals would not change their perceived risk after stage 3, when the geophysical information is first introduced. The formulation of this hypothesis was proposed because it is assumed that the focus group participants did not have expertise nor did the geophysical information present any new information. Most of the participants followed this pattern; however, participants 1, 8 and 9 updated their subjective probability at all stages after 3, i.e., as the more highly technical geophysical information had been introduced. It can be inferred that the highly technical geophysical information induced a change in risk perception in these individuals. This induced change may have resulted from students having prior knowledge of geophysics, and did not believe geophysical information was useful. Participants 8 and 9 revealed a subjective probability at one of the extreme values (i.e., <1 and 98, respectively). This could be a result of a propensity to hold strong opinions, or prior knowledge of debris flows within the Boulder area. In both cases, the highly technical geophysical information led them to an even more extreme probability assignment. It is unclear whether these individuals hold that the highly technical geophysical information has provided such rich, clear evidence that they can confidently state that a debris flow is virtually certain to occur, or virtually certain not to occur, within a year. Alternatively, the extreme probability assignments might just be a statement that they believe they have a good grasp on the physical factors that control the occurrence of a debris flow. In other words, their extreme values could be representative

of the confidence they have in setting a risk level, rather than representative of the actual risk level itself. It seems difficult to imagine that the geophysical evidence presented here was so compelling as to induce someone, who was somewhat on the fence before exposure to any geophysical information, into believing that a debris flow was virtually certain to occur within a year.

Participant 1 was not able to assess his or her risk of debris flows after exposure to highly technical geophysical information was presented in stages 4 and 5. In other words, it appears that the geophysical information actually caused this person to lose his or her grasp on the risk of debris flows that this person reported after looking at the photographs and hearing the general site description in stages 1 and 2. In other words, it appears that the geophysical information caused this person to distrust their common general knowledge about debris flows. This could have been due to the overwhelming nature of the highly technical geophysical information. Another interpretation is that this person simply misread the instructions and made a risk assignment solely on the highly technical geophysical information, when actually the participants were instructed to update their previously-held risk assignments.

Participants 2-7 did not change their subjective risk probability upon exposure, after stage 3, to the highly technical geophysical information. This could be attributed to a lack of understanding of the geophysical information, or an understanding that did not affect their perceived risk, or that the geophysical information was ignored due to lack of interest in following technical argumentation. In general, a presenter may also be seen as untrustworthy or unknowledgeable, but this is not thought to be a factor here, as the

presenter was a peer colleague with roughly the same level of educational background as each of the participants. For this study, individuals may have had a bias for their own expertise or understanding of debris flows, and these individuals may believe that geophysical information, no matter how it is presented, is inherently unable to provide useful information about debris flow hazard assessment. In other words, some participants may have been so affected by the inherent uncertainty of geophysical information as to simply ignore all of it.

The descriptive responses indicated that individuals mostly understood the information presented during stages 1 and 2, as expected. Topography, rainfall measures and photographs of debris flow destruction were dominant in directing individuals to choose particular probabilities. Also noted was a desire for more background information about the debris flow history of the area. The geophysical information induced a more varied response. Some individuals after stage 3 noted that the SRC maps confirmed their previous probability assignment, whereas other individuals completely disagreed with the interpretation of the SRC maps. Some individuals saw the geophysical information as simply "clouding the effect" of information presented during stages 1 and 2. After stage 4, some individuals began to lose interest and understanding of the geophysical material. Some individuals wrote "I did not fully understand how the methods or raw results tells me the likelihood of a debris flow". Also noted, was that the geophysical information was "nothing new" (see Appendix). These individuals did not update their subjective debris flow risk probability after the highly technical geophysical information was presented. However, the individuals on the extreme ends of probability noted that "the correlation of

high-low resistivity with relation to the varied lithology" was enough to change his or her risk probability. Perhaps in these cases the extreme probability assignments were a reflection of a good command of the general causative factors of debris flows, rather than an actual assessment of the stability of the slopes around Boulder. After stage 5, only one individual viewed the most highly technical information as useful to his or her probability assignment.

The inferences from the risk perception survey can be summed up by:

- Results followed the hypothesis – Most individuals would not update their subjective probabilities after introduction to geophysical information (after stage 3).

- Most individuals were unaffected by the geophysical information and it did not change their perception of the risk of a debris flow, as expressed after exposure to the general information of stages 1 and 2.

- Individuals with extreme subjective probabilities, in either direction, seemed to further harden their viewpoint when introduced to highly technical geophysical information.

- Some participants may become overwhelmed with highly technical geophysical information and lose an ability to assess their perceived risk, even with a base of common general knowledge.

- Individuals with specific technical backgrounds tend to give more credence to information that is relevant to their own area of expertise.

- The greater the technical level of information presented, the less the individuals used the information to update prior knowledge.

This risk perception survey attempted to elicit individuals' subjective probability of debris flow risk following introduction to varying technical levels of information about ERT imaging of susceptible slopes. The results show a clear distinction between each participant by not only the perceived debris flow subjective risk probability, but the probability value itself. The results show that even in small sample sizes with individuals of similar educational attainment, subjective probability varies widely. With sample size of nine participants ($N$=9), it is difficult to come to any firm conclusions concerning what level of technical detail, if any, is useful for educating the general public using geophysical information. Rather, this study gives insight and guidance toward the development of a larger, more carefully-designed risk perception study. This is an essential step to incorporating geophysical information into strategies for educating the public living in debris flow susceptible areas.

REFERENCES

AGI. (2009). Instruction manual for EarthImager™ 2D version 2.4.0. Advanced Geosciences, Inc, Austin, Texas.

Anderson, K. G., and Jackson, R. (1992). A comparison of the solutions of some proposed equations of motion of granular materials for fully developed flow down inclined planes. *Journal of Fluid Mechanics, 241*(-1), 145. doi:10.1017/s0022112092001988

Benda, L. E., and Cundy, T. W. (1990). Predicting deposition of debris flows in mountain channels. *Canadian Geotechnical Journal*, 27(4), 409-417.

Bogoslovsky, V. A., Ogilvy, A. A., and Strakhova, N. A. (1977). Magnetometric and electrometric methods for the investigation of the dynamics of landslide processes. *Geophysical Prospecting, 25*(2), 280-291.

Boulder County. (n.d.). Retrieved April 22, 2015, from http://www.bouldercounty.org/pages/default.aspx

Boonchaisuk, S., Vachiratienchai, C., and Siripunvaraporn, W. (2008). Two-dimensional direct current (DC) resistivity inversion: Data space Occam's approach. *Physics of the Earth and Planetary Interiors*, 168(3-4), 204-211.

Braddock, W. A., and Eicher, D. L. (1962). Block-Glide Landslides in the Dakota Group of the Front Range Foothills, Colorado. *Geological Society of America Bulletin, 73*(3), 317.

Bridge, R. (2004). *The geology of Boulder County*. Boulder, CO: Lone Eagle Publications.

Cameron, T. A. (2005). Updating subjective sisks in the presence of conflicting information: an application to climate change. *Journal of Risk and Uncertainty*, 30(1), 63–97.

Carey, J., and Petley, D. (2014). Progressive shear-surface development in cohesive materials; implications for landslide behaviour. *Engineering Geology*, 177, 54-65. doi:10.1016/j.enggeo.2014.05.009

Charness, G., Gneezy, U., and Imas, A. (2013). Experimental methods: eliciting risk preferences. *Journal of Economic Behavior & Organization*, 87, 43-51

Clark, J. A., and Page, R. (2011). Inexpensive geophysical instruments supporting groundwater exploration in developing nations. *Journal of Water Resource and Protection*, 03(10), 768-780. doi:10.4236/jwarp.2011.310087

Coe, J. A., Kean, J. W., Godt, J. W., Baum, R. L., Jones, E. S., Gochis, D. J., and Anderson, G. S. (2014). New insights into debris flow hazards from an extraordinary event in the Colorado Front Range. *GSA Today*, 24(10), 4-10.

Dahlin, T. (2001). The development of DC resistivity imaging techniques. *Computers & Geosciences*, 27(9), 1019-1029. doi:10.1016/s0098-3004(00)00160-6

Daily, W., and Owen, E. (1991). Cross-borehole resistivity tomography. *Geophysics*, 56(8), 1228-1235.

Degroot-Hedlin, C., and Constable, S. (1990). Occam's inversion to generate smooth, two-dimensional models from magnetotelluric data. *Geophysics*, 55(12), 1613-1624.

Dostál, I., Putiška, R., and Kušnirák, D. (2014). Determination of shear surface of landslides using electrical resistivity tomography. *Contributions to Geophysics and Geodesy, 44*(2).

Ellen, S. D., and Fleming, R. W. (1987). Mobilization of debris flows from soil slips, San Francisco Bay region, California. *Debris Flows/Avalanches: Process, Recognition, and Mitigation Reviews in Engineering Geology*, 31-40.

Erginal, A. E., Öztürk, B., Ekinci, Y. L., and Demirci, A. (2008). Investigation of the nature of slip surface using geochemical analyses and 2-D electrical resistivity tomography: A case study from Lapseki area, NW Turkey. *Environmental Geology Environ Geology, 58*(6), 1167-1175.

ESRI 2015. ArcGIS Desktop: Release 10.3. Redlands, CA: Environmental Systems Research

Everett, M. E. (2013). *Near-Surface Applied Geophysics*. Cambridge University Press Textbooks.

Friedman, S. P. (2005). Soil properties influencing apparent electrical conductivity: A review. *Computers and Electronics in Agriculture*, 46(1-3), 45-70.

Furman, A., Ferre, T. P., and Warrick, A. W. (2003). A sensitivity analysis of electrical resistivity tomography array types using analytical element modeling. *Vadose Zone Journal*, 2(3), 416-423. doi:10.2113/2.3.416

Godio, A., Strobbia, C., and Bacco, G. D. (2006). Geophysical characterisation of a rockslide in an alpine region. *Engineering Geology*, 83(1-3), 273-286. doi:10.1016/j.enggeo.2005.06.034

Godt, J. W., and Coe, J. A. (2007). Alpine debris flows triggered by a 28 July 1999 thunderstorm in the central Front Range, Colorado. *Geomorphology*, 84(1-2), 80-97. doi:10.1016/j.geomorph.2006.07.009

Iverson, R. M., Reid, M. E., and Lahusen, R. G. (1997). Debris flow mobilization from landslides 1. *Annual Review of Earth and Planetary Sciences*, 25(1), 85-138.

Jakob, M., and Hungr, O. (2005). *Debris flow hazards and related phenomena*. Berlin: Springer.

Johnson, K. A., and Sitar, N. (1990). Hydrologic conditions leading to debris flow initiation. *Canadian Geotechnical Journal*, 27(6), 789-801.

Konishi, Y. and K. Adachi. (2011). A framework for estimating willingness-to-pay to avoid endogenous environmental risks. *Resource and Energy Economics*, 33: 130–154.

Kunreuther, H., Novemsky, N., and Kahneman, D. (2001). Making low probabilities useful. *Journal of Risk and Uncertainty*, 23(2), 103-120.

Lapenna, V., Lorenzo, P., Perrone, A., Piscitelli, S., Rizzo, E., and Sdao, F. (2005). 2D electrical resistivity imaging of some complex landslides in Lucanian Apennine chain, southern Italy. *Geophysics, 70*(3).

Lee, C., Zeng, L., Hsieh, C., Yu, C., and Hsieh, S. (2012). Determination of mechanisms and hydrogeological environments of Gangxianlane landslides using geoelectrical and geological data in central Taiwan. *Environmental Earth Sciences, 66*(6), 1641-1651.

Lindell, M. K., and Earle, T. C. (1983). How close is close enough: public perceptions of the risks of industrial facilities. *Risk Analysis, 3*(4), 245-253.

Loke, M., Acworth, I., and Dahlin, T. (2003). A comparison of smooth and blocky inversion methods in 2D electrical imaging surveys. *Exploration Geophysics*, 34(3), 182.

Loke, M. H., and Barker, R. D. (1995). Least-squares deconvolution of apparent resistivity pseudosections. *Geophysics, 60*(6), 1682-1690.

Loke, M.H. (1999). *Electrical imaging surveys for environmental and engineering studies*. User's Manual for Res2dinv.

Mejía-Navarro, M., Wohl, E. E., and Oaks, S. D. (1994). Geological hazards, vulnerability, and risk assessment using GIS: Model for Glenwood Springs, Colorado. *Geomorphology and Natural Hazards*, 331-354.

Merritt, A., Chambers, J., Wilkinson, P., West, L., Murphy, W., Gunn, D., and Uhlemann, S. (2016). Measurement and modelling of moisture—electrical resistivity relationship of fine-grained unsaturated soils and electrical anisotropy. *Journal of Applied Geophysics*, 124, 155-165.

NOAA. (n.d.). Boulder, Colorado weather and climate. Retrieved November 9, 2015, from http://www.esrl.noaa.gov/psd/boulder/Boulder.mm.precip.html

Perrone, A., Lapenna, V., and Piscitelli, S. (2014). Electrical resistivity tomography technique for landslide investigation: A review. *Earth-Science Reviews*, 135, 65-82.

Radbruch-Hall, D.H., Colton, R.B., Davies, W.E., Lucchitta, Ivo, Skipp, B.A., and Varnes, D.J. (1982). Landslide overview map of the conterminous United States. *Geological Survey Professional Paper 1183*, U.S. Geological Survey, Washington.

Reid, M. E., and Iverson, R. M. (1992). Gravity-driven groundwater flow and slope failure potential: 2. Effects of slope morphology, material properties, and hydraulic heterogeneity. *Water Resources Research*, 28(3), 939-950. doi:10.1029/91wr02695

Runnells, D. D. (1980). *Boulder, a sight to behold: Guidebook*. Boulder: Johnson Pub.

Shaw, W. (in press). Environmental and Natural Resource Economics Decisions under Risk and Uncertainty: A Survey. *International Review of Environmental and Resource Economics.*

Steelman, T. A., and Mccaffrey, S. (2012). Best practices in risk and crisis communication: Implications for natural hazards management. *Natural Hazards*, 65(1), 683-705.

Tabbagh, A., Panissod, C., Guérin, R., and Cosenza, P. (2002). Numerical modeling of the role of water and clay content in soils' and rocks' bulk electrical conductivity. *Journal of Geophysical Research: Solid Earth, 107*(B11).

Udphuay, Suwimon (2008). 3-D electrical resistivity tomography for cliff stability assessment at Pointe du Hoc in Normandy, France. Doctoral dissertation, Texas A&M University. Available electronically from: http://hdl.handle.net/1969.1/ETD-TAMU-2008-12-155.

USGS. (n.d.). The national map. Retrieved January 23, 2016, from http://nationalmap.gov/

Vallee, D. (2014). *The record front range and eastern Colorado floods of September 11-17, 2013* (pp. 1-84) (United States of America, National Oceanic and Atmospheric Administration, National Weather Service). Silver Spring, MD.

Viscusi, W. K. (1993). The value of risks to life and health. *Journal of Economic Literature*, 1912-1946.

Waagé, K. M. (1955). *Dakota group in Northern Front Range Foothills, Colorado*. Washington: United States Government Printing Office.

Wannamaker, P., Stodt, J., and Rijo, L. (1987). A stable finite element solution for two-dimensional magnetotelluric modelling. *Geophysics Journal International*, 88 (1).

# APPENDIX

## SPATIAL RESISTANCE CHANGE MATLAB CODE

```matlab
% Plot 2D Resistivity Data into grid and create hazard map.  This program
% uses triangulation to retain original resistivity profile. The primary
% inversion technique used is the Smooth model inversion.
% Created by Daniel Tebo, MS student at Texas A&M

% Tr=0.85; % Transparency of image
X = VarName1; %X-Coordinate of data imported from AIG
Y = VarName2; %Y-Coordinate of data imported from AIG
C = VarName3; %Resistivity data imported from AIG
Hr=100; % Limit for Magnitude of change in Resistivity
%Rt1=10,Rt2=50,Rt3=100,Rt4=150,Rt5=200,Rt6=300
electsp=2; % electrode spacing
s=0.8; % Shrink factor for boundary function (0.5 for B4, 0.8 for B2,
etc.)


% Locate the boundary of the profile (no superfluous information)!
xyz = [X Y]; % Combine X,Y Coordinates
K = boundary(Y,X,s); % Map boundary of true data
xy = [X(K) Y(K)]; % Combine X,Y Coordinates of boundary
for i = 2:size(K) % Loop to create indicies of boundary
    xk(i) = K(i-1);yk(i) = K(i);
    xk(length(K)) = K(length(K));yk(length(K)) = 1;
end
tr = [xk' yk'];
tr(1,:)=[];
tr(length(K)-1,:)=[K(length(K)-1) K(1)];% Boundary constraint for
triangulation

%%%%%%%%%%%%%%%%%%%%%%%%%%%%%%%%%
dt = delaunayTriangulation(X,Y,tr);% delaunay triangulation of
resistivity profile.
%%%%%%%%%%%%%%%%%%%%%%%%%%%%%%%%%

cl = dt.ConnectivityList;% Find the triangle indicies
IO = isInterior(dt);% locate points within triangulation

%-Sorting for SRC loop--------------------------------
% This sorts the data into spatially adjacent cells
[srt, sri] = sort(X,1);
ixc = srt==0;
xc = sum(ixc(:));
lngth = length(X)/xc;
ytr = reshape(sri,[xc,lngth]);
yy = Y(ytr);
xx = X(ytr);
```

```matlab
cc = C(ytr);
MRC5 = zeros(xc,lngth);

% This loop calculates the magnitude of spatial resistance change (ohm-
m/m)
for i = 2:xc-1
    for j = 2:lngth-1
        MRC5(i,j) = sqrt((((abs(cc(i,j+1)-cc(i,j-1)))/(abs(xx(i,j-1))-
xx(i,j+1)))^2)...
             +((abs(cc(i+1,j)-cc(i-1,j))/(abs(yy(i+1,j)-yy(i-1,j))))^2));
        % Limit to maximum amount of resistance change within profile
        if MRC5(i,j)>=Hr;
            MRC5(i,j)=Hr;
        end
        % -------------------------------------------------------
    end
end

%----Boundary conditions---------------------------------------
% MRC5(1,:)=MRC5(2,:);
% MRC5(xc,:)=MRC5(xc-1,:);
% MRC5(:,1)=MRC5(:,2);
% MRC5(:,lngth)=MRC5(:,lngth-1);

%-----Reshape MRC5 back to original format-----------------------
mrc5 = reshape(MRC5,[length(X),1]);% Reshape matrix to vector
[org, jpg] = sort(sri);% sort vector and gather indices
mrc5 = mrc5(jpg);% Put SRC data back to original format
ytr = yy(jpg);

%-----load Colormaps---------------------------
load ('mycolormap'); % Cmap
load ('mycolormap2'); % map
load ('mycolormap3'); % map2
load ('mycolormap4'); % map3
load ('mycolormap5'); %map4
%----------Add electrode positions-----------------------------
elex = zeros(1,56);
eley = zeros(1,56);
for i=1:electsp:length(xx)
    elex(i)=xx(1,i);
    eley(i)=yy(1,i);
end
%-------------------------------------------------------------

R2=log(C(:,:)); % Plot resistivity in logarithmic scale

%------Add Transparency to figure---------------------------------
ypt = yy';
Tr=zeros(length(yy),xc);
for i=1:length(yy)
```

```matlab
    for j=1:xc
        Tr(i,j)=abs(ypt(i,j))/abs(ypt(i,1));
    end
end
Tr = Tr';
ntr = Tr(jpg);
scaled = ntr - min(ntr);
scaled = scaled / max(scaled);
scaled = sqrt(scaled);


%-----Figures-------------------------------
figure(1) % Plots original inverted resistivity profile
Contours=[10 30 100 300 1000];
h(1)=trisurf(dt(IO, :),dt.Points(:,1),
dt.Points(:,2),R2,'EdgeColor','none');
hold on
h(2)=plot(elex,eley,'+k','LineWidth',1.5);
alpha (scaled)
% shading interp
xlabel('Distance From Starting Electrode (meters)','FontSize',12)
ylabel('Elevation (meters)','FontSize',12)
legend(h(2),'ELECTRODE','Location','northeast','FontSize',14)
view([0 0 90]);
caxis(log([Contours(1) Contours(length(Contours))]));
h=colorbar('FontSize',12,'YTick',log(Contours),'YTickLabel',Contours,'Loc
ation','southoutside');
h.Label.String='Resistivity (ohm-m)';
h.Label.FontSize=12;
% colormap(Cmap/255)
colormap(jet)
axis equal
xlim([min(X) max(X)])
ylim([min(Y) max(Y)])
title('2D Resistivity Profile - Transect B6','FontSize',16)
grid on

figure(2)% Plots location of datum points in X,Y coordinates
plot(X,Y,'.')

figure (3)% Plots spatial resistance change (SRC)
Contours=[10 30 100 300 1000];
h(1)=plot(elex,eley,'+k','LineWidth',1.5);
hold on
h(2)=trisurf(dt(IO, :),dt.Points(:,1),
dt.Points(:,2),mrc5,'EdgeColor','none');
% alpha(scaled)
shading interp
% colormap(hot)
colormap(map4/255)% adds RGY to profile for hazard identification
xlabel('Distance From Starting Electrode (meters)','FontSize',12)
ylabel('Elevation (meters)','FontSize',12)
legend(h(1),'Electrode','Location','northeast','FontSize',14)
```

```matlab
view([0 0 90]);
h=colorbar('Location','southoutside');
h.Label.String='Spatial Resistance Change (ohm-m/m)';
h.Label.FontSize=12;
kmin=min(mrc5(:));
kmax=max(mrc5(:));
%---------changing Hr value-------------------------
if Hr==10
    Rt1 = [kmin 2 4 6 8 kmax];
    h.Ticks=Rt1;
    h.TickLabels={'0','2','4','6','8','>10'}; % Hr=10
elseif Hr==50
    Rt2 = [kmin 10 20 30 40 kmax];
    h.Ticks=Rt2;
    h.TickLabels={'0','10','20','30','40','>50'}; %Hr = 50
elseif Hr==100
    Rt3 = [kmin 20 40 60 80 kmax];
    h.Ticks=Rt3;
    h.TickLabels={'0','20','40','60','80','>100'}; %Hr = 100
elseif Hr==150
    Rt4 = [kmin 25 50 75 100 125 kmax];
    h.Ticks=Rt4;
    h.TickLabels={'0','25','50','75','100','125','>150'}; %Hr = 150
elseif Hr==200
    Rt5 = [kmin 50 100 150 kmax];
    h.Ticks=Rt5;
    h.TickLabels={'0','50','100','150','>200'}; % Hr = 200
elseif Hr==300
    Rt6 = [kmin 50 100 150 200 250 kmax];
    h.Ticks=Rt6;
    h.TickLabels={'0','50','100','150','200','250','>300'}; % Hr = 300
elseif Hr==75
    Rt7 = [kmin 15 30 45 60 75];
    h.Ticks=Rt7;
    h.TickLabels={'0','15','30','45','60','75'}; % Hr = 75
end
%------------------------------------------------------
axis equal
xlim([min(X) max(X)])
ylim([min(Y) max(Y)])
title('2D Susceptibility Profile - Debri-Flow/Landslide Slip Surface
(Transect B6)','FontSize',16)
grid on
```

*(Responses are numbered by participant (i.e. participant 1 = 1))*

# Perceived Debris-Flow Risk Survey

**_Instructions:_** *For each break in the PowerPoint Presentation, Rank **_YOUR_** perceived debris-flow risk, as if you lived downslope of the risk assessment area (using the information presented). Please assess your perceived risk on a scale of 0-100.*

**_A perceived risk of 0 indicates no risk at all, and a perceived risk of 100 indicates the highest perceived risk._**

## Break 1:

On a scale of 0-100, what is your perceived risk using the information presented.

1. 100
2. 10
3. 40-50
4. 60
5. <5%
6. 70
7. (Boulder) greater than 20. Due to topography/precipitation in the region, plus one previous event.
8. 50%
9. 85

What information directed you to choose this perceived risk level (if any)?

1. Knowing where Boulder is situated (high susceptibility due to topography and rainfall)

+ Experience of living in such area

+ongoing change in vegetation, climate, existing management

2. How flood frequency is measured, i.e. 100 vs 500 year flood.
3. The images of the damages caused by debris flows raised it, but not knowing about where this is taking place and the nature of the topography lowered it.
4. The overall map showed the locations with high topography have moderate to high chance of debris flows. As well as the 500 year flood which showed debris flows do happen.
5. The cause of 2 debris flows was a 500 yr flood, which is not a common occurrence.
6. It looks like lots of debris flows occur there! I would have said 100, but I know it might not happen next year. It may happen a few years from now.
7. Boulder is in an area of high topography and has higher amount so precipitation, two categories. It's had one recent event, but at this point that all we know about. Could be a 1 in 500 year event with the flood.
8. Topography & history
9. The high topography, moderate to high relief and the cyclicity of rainfall in the Boulder area. Growing population building homes on steep slopes.

## If your risk perception did not change, why?

1. It was at 100% earlier as well.
2. It did not change because no new (to me) information was provided.
3. Limited background information on the area/region.
4. –
5. 1st prob
6. It did change – went up because I didn't know before that debris flows were so common there. I do know now!
7. –
8. I had no idea what caused debris flow and whether Boulder was a susceptible area or not.
9. No, my probability did not change.

# Break 2:

On a scale of 0-100, what is your perceived risk using the information presented.

1. 75 – 100%
2. 10
3. 50-55
4. 65
5. <5%
6. 75
7. More than 40. More information has been given but at the moment, rainfall seems to be the driving force. For just one 500 year flood.
8. 30
9. 95

What information directed you to choose this perceived risk level (if any)?

1. Along a particular slope, my risk will depend on my knowledge of lithology + my observation of land cover, land management.
2. I chose to keep my previous estimate because the rainfall event was an outlier, so possibility is still low.
3. Increased because more information/background, climate trends
4. Susceptibility map. The rainfall chard indicated that the debris flows were caused by abnormal rainfall. So the risk initially is less but due to the susceptibility map indicating areas of high potential for debris flows, the probability is higher.
5. The rainfall distribution showed 9" of rainfall, which is well above average/normal. Assuming next year is a normal rainfall year, I have not seen evidence that the risk is high.
6. The geophysical survey data, where it was collected, showed high probability of a debris flow in the area.
7. Slopes are colluvium/mass wasting.  High elevation (gravity). Previous debris flows and numerous. Survey shows region at higher susceptibility.
8. Though topography is there, rainfall is usually not.

9. The combination of the complex geologic setting and high topography. Greater human present in Boulder area.

If your risk perception did not change, why?

1. –
2. No new information was provided.
3. It did
4. –
5. All the information reinforced that the debris flows were freak events based on the record rain.
6. –
7. –
8. It did not change. Knowing the rainfall patterns changed it.
9. From the information provided, the stage is set from debris flow activity in Boulder.

# Break 3:

On a scale of 0-100, what is your perceived risk using the information presented.

1. Same!
2. 10
3. 50
4. 75
5. 15%
6. 75
7. Still at 40. Still need the triggering event (rainfall).
8. 10%
9. 95

## What information directed you to choose this perceived risk level (if any)?

1. Specific to the site, I'd base my probability more on the calona… (not sure what word that is).
2. No new information – yes. There are potential slip surfaces, but what is the slope?
3. Data for break 3 seemed to focus on data quality issue instead of hazards. Meaning the same data is clouding the effect.
4. Indications on B2 & B4 on the spatial resistance change map showed areas that can cause slips do occur between rock units if heavy rainfall.
5. I assume the survey was conducted under normal conditions. No recent record rainfalls and areas of "risk"/susceptibility to debris flows were identified.
6. The slip surface areas picked up the ERT affirmed my previous number of 75.
7. ERT/ change in lithology (slip surface between sand and clay). Map showing variability in the survey-line B2.
8. The composition of the soil as explained is not as prone to debris flow. So combined with low average rainfall, not so likely.
9. The subsurface ERT data displays an evident slip surface (failure plane)

## If your risk perception did not change, why?

1. –
2. I want to know the slope of the area and see spatially where the potential slip surfaces are. Also, what had the weather been before/during your sampling? What time of year was it?
3. –
4. –

5. –
6. Because there was no new information that I understood very well.
7. Other lines showed less variability than expected. B2 has the most unstable, while the other 3 lines showed no real cause of concern. Is the edge of the other slide known? Could be useful to know when presenting for concern.
8. –
9. The probability is high because, obvious slope morphology features (failure plane) are present. These slopes are potentially active.

# Break 4:

On a scale of 0-100, what is your perceived risk using the information presented.

1. Cannot say!
2. 10
3. 50
4. 75
5. 15%

6. 75
7. Still around 40 which information present.
8. <1%
9. 95

## What information directed you to choose this perceived risk level (if any)?

1. Specific to my location in Boulder. I'd need more information on/interpretation of ERT.
2. I see conditions were assumed unsaturated and sampling was done in March. This gives more information, but I think probability is still low because it seems dependent on a significant rainfall.
3. Side note: on the B2 resistivity section, on the figure in powerpoint annotate where trails cross to avoid confusion.
4. Really the information already presented
5. I did not fully understand how the methods or raw results tells me the likelihood of a debris flow.
6. Nothing new during this section of the presentation
7. Resistivity cross sections
8. The method to measure resistivity corroborates the previous set of information. It would have to rain record levels again to get debris flow.
9. The correlation of high-low resistivity with relation to the varied lithology.

## If your risk perception did not change, why?

1. It tells me how to go about looking for debris flow, but shows of lot of uncertainty… does not translate the information to what I need to know!
2. I am wondering what influence snowmelt has on soil saturation and slope stability. Do debris flows occur with snowmelt? My response has not changed because my initial assumptions are holding true.
3. My probability would increase for the slope mentioned, however the new material shown in break 4 did not lead me to feel more at risk for debris flows or mass movement in the "slides of boulder". Just local to this slope.
4. The information shown didn't indicate any information about potential of a debris flow occurring. The information gave knowledge as to what the subsurface could be.
5. I did not perceive any new "risk" information from this section.

6. Because nothing presented seemed to say anything different, or as easy to understand, from the previous slides.
7. Methods didn't really help in determining risk factors. It's good to explain what you were doing, but it didn't aid me in determining risk.
8. –
9. My guess for probability remains high, because this data reinforces the unstable environment in Boulder.

# Break 5:

On a scale of 0-100, what is your perceived risk using the information presented.

1. Cannot say!
2. 10
3. 50
4. 75
5. 15%
6. 75
7. Still around 40 based on information
8. <1%
9. 98

What information directed you to choose this perceived risk level (if any)?

1. I was looking for some ground trothing of the inversion models… to test some debris flow hypotheses.
2. –
3. The general public will not understand this section but it makes a great point to show the depth of work that goes into a geophysical model and shown peoples attention to risk.
4. The information shown previously
5. Explanation of model and calculations was not clear (may be lack of knowledge on subject). Knowing how risk/maps were determined did not increase my perceived risk for my "home" at the base of the slope.
6. Nothing new
7. SRC (Spatial resistance change)
8. –
9. The math and analysis behind the ERT data. The display showing the difference between the methods directed me to choose this probability.

## If your risk perception did not change, why?

1. This information was very method focused. Was not helpful at all in understanding the processes I need to know to assess the risk.
2. It has not changed because I want to know more about the surface and its relationship with the subsurface.  I feel I have an incomplete picture, so my perception has changed the same throughout.
3. Provided background to methodology but did not provide new information regarding "additional" risk/susceptibility
4. The information presented gave credence to your models but did not change what the initial figures shown. So no change in probability from previous.
5. The new info was only about how the orig. risk was calculated. No new information regarding how likely a debris flow is to occur was presented.
6. Because you lost me. I like to know the scientists conclusions on matters like this, but I don't care so much about how you got to these conclusions (maybe I should, but it's over my head, so meh… it doesn't matter).
7. Techniques and the procedure explaining how you arrived at your model are very important, but not sure it adds more to what was already presented. I could tell from the earlier slides the area is somewhat stability. The reason I didn't give this a higher probability is because the other half (rainfall) is unknown.

8. The change of model selection is irrelevant to the propensity of the region to actual debris flow.
9. –